

## Upflows in the Upper Solar Atmosphere

Hui Tian<sup>1,2</sup>  · Louise Harra<sup>3,4</sup>  ·  
Deborah Baker<sup>5</sup>  · David H. Brooks<sup>6</sup>  ·  
Lidong Xia<sup>7</sup> 

© Springer ●●●

**Abstract** Spectroscopic observations at extreme- and far-ultraviolet wavelengths have revealed systematic upflows in the solar transition region and corona. These upflows are best seen in the network structures of the quiet Sun and coronal holes, boundaries of active regions, and dimming regions associated with coronal mass ejections. They have been intensively studied in the past two decades because they are likely to be closely related to the formation of the solar wind and heating of the upper solar atmosphere. We present an overview of the characteristics of these upflows, introduce their possible formation mechanisms, and discuss their potential roles in the mass and energy transport in the solar atmosphere. Although past investigations have greatly improved our understanding of these upflows, they have left us with several outstanding questions and unresolved issues that should be addressed in the future. New observations from the *Solar Orbiter* mission, the *Daniel K. Inouye Solar Telescope* and the *Parker Solar Probe* will likely provide critical information to advance our understanding of the generation, propagation, and energization of these upflows.

---

✉ H. Tian  
[huitian@pku.edu.cn](mailto:huitian@pku.edu.cn)

<sup>1</sup> School of Earth and Space Sciences, Peking University, Beijing 100871, China

<sup>2</sup> Key Laboratory of Solar Activity, National Astronomical Observatories, Chinese Academy of Sciences, Beijing 100012, China

<sup>3</sup> PMOD/WRC, Dorfstrasse 33, 7260 Davos Dorf, Switzerland

<sup>4</sup> ETH-Zürich, Hönggerberg Campus, Zürich, Switzerland

<sup>5</sup> Mullard Space Science Laboratory, University College London, Holmbury, St. Mary, Dorking, Surrey, KT22 9XF, UK

<sup>6</sup> College of Science, George Mason University, 4400 University Drive, Fairfax, VA 22030, USA

<sup>7</sup> Shandong Provincial Key Laboratory of Optical Astronomy and Solar-Terrestrial Environment, Institute of Space Sciences, Shandong University, Weihai, 264209 Shandong, China

**Keywords:** Active Regions, Velocity Field; Coronal Holes; Coronal Mass Ejections, Low Coronal Signatures; Heating, Coronal; Spectral Line, Broadening

## 1. Introduction

The upper solar atmosphere consists of the corona and transition region (TR), spanning a temperature range from about  $3 \times 10^4$  to several million Kelvin. In such a hot environment, atoms are often highly ionized and produce hundreds of strong emission lines mainly at extreme-ultraviolet (EUV) and far-ultraviolet (FUV) wavelengths ( $\approx 100 - 1700 \text{ \AA}$ ). In the past quarter century, dedicated observations with several EUV/FUV spectrographs, particularly the *EUV Imaging Spectrometer* (EIS: Culhane et al., 2007) onboard *Hinode* (Kosugi et al., 2007), the *Interface Region Imaging Spectrograph* (IRIS: De Pontieu et al., 2014), the *Solar Ultraviolet Measurements of Emitted Radiation* (SUMER: Wilhelm et al., 1995; Lemaire et al., 1997), and the *Coronal Diagnostic Spectrometer* (CDS: Harrison et al., 1995) onboard the *Solar and Heliospheric Observatory* (SOHO: Domingo, Fleck, and Poland, 1995), have greatly improved our understanding of various types of dynamic activity in the upper solar atmosphere.

Signatures of outflows or upflows, i.e. blue shifts of spectral lines, have been frequently reported from spectroscopic observations with these facilities. In this review, we focus on the systematic and pervasive upflows observed primarily with the aforementioned spectrographs. Sporadic upflows/outflows such as coronal mass ejections and coronal jets are not discussed in this review. These systematic upflows have been one focus of investigation in the past two decades, mainly because they are likely to be related to the formation of the solar wind. In addition, these upflows are expected to contribute to the mass and energy transport in the solar atmosphere, and thus may play an important role in coronal heating.

Here we present a review on both observational and theoretical investigations of these upflows. We first discuss upflow signatures in the quiet Sun and coronal holes in Section 2, then provide a detailed introduction to the coronal-upflow phenomenon at active-region (AR) boundaries in Section 3. Section 4 describes characteristics of the upflows identified from regions of coronal dimmings induced by coronal mass ejections (CMEs). Finally, we summarize the major findings about these upflows and briefly discuss future perspectives in Section 5.

## 2. Upflows from the Quiet Sun and Coronal Holes

### 2.1. Quiet-Sun Regions

It has been known since the 1970s that emission lines formed in the TR, such as C IV 1548  $\text{\AA}$  formed at a temperature of  $\approx 10^5 \text{ K}$  under ionization equilibrium, are redshifted by a few  $\text{km s}^{-1}$  on average in the quiet Sun (e.g. Doschek, Feldman, and Bohlin, 1976). The red shift is obviously larger in network regions compared to internetwork regions (Figure 1). With the capability of observing hundreds of strong emission lines formed in a wide range of temperatures, the SUMER

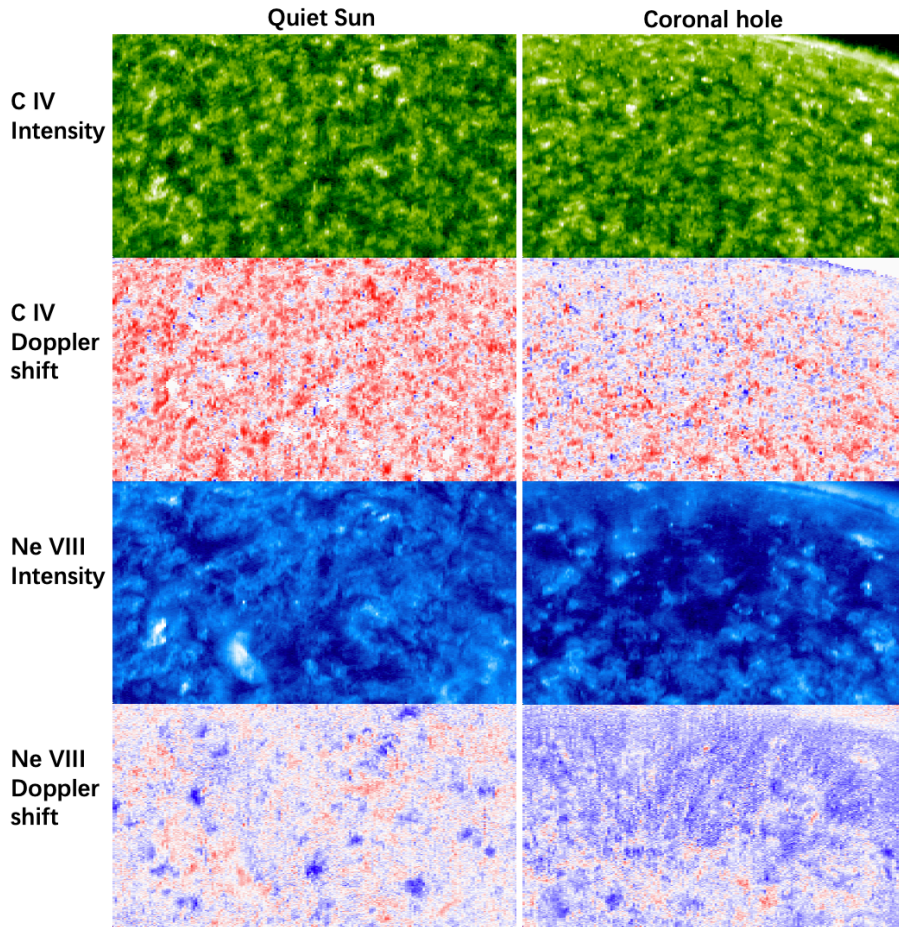


**Figure 1.** Intensity and Doppler shift images of C IV 1548 Å and Ne VIII 770 Å. Blue and red colors in the Dopplergrams indicate blue shifts and red shifts, respectively. These images correspond to a field of view (FOV) of  $540'' \times 300''$ , and are taken from the SUMER Image Database: <http://www2.mps.mpg.de/projects/soho/sumer/text/s029601.html>. The same datasets have been analyzed by Dammasch et al. (1999) and Hassler et al. (1999).

spectrometer allowed detailed investigations of the Doppler shift as a function of the line-formation temperature. SUMER observations revealed a clear dependence of the Doppler shift on temperature, i.e. the average red shift increases with temperature and peaks around  $2 \times 10^5$  K (or  $\log T = 5.3$ ) (e.g. Peter and Judge, 1999; Stucki et al., 2000; Dadashi, Teriaca, and Solanki, 2011). As the temperature continues to increase, the average red shift decreases and turns into a blue shift above  $\approx 5 \times 10^5$  K. This trend can be clearly seen from Figure 2.

The change from downflow (i.e. red shifts of spectral lines) dominance to up-flow dominance was unambiguously established from observations of the strong Ne VIII 770 Å line, which is formed at  $\approx 6.5 \times 10^5$  K in the upper TR or lower corona. Under the assumption of zero average Doppler shift above the solar limb, Dammasch et al. (1999) determined a rest wavelength of  $770.428 \pm 0.003$  Å for

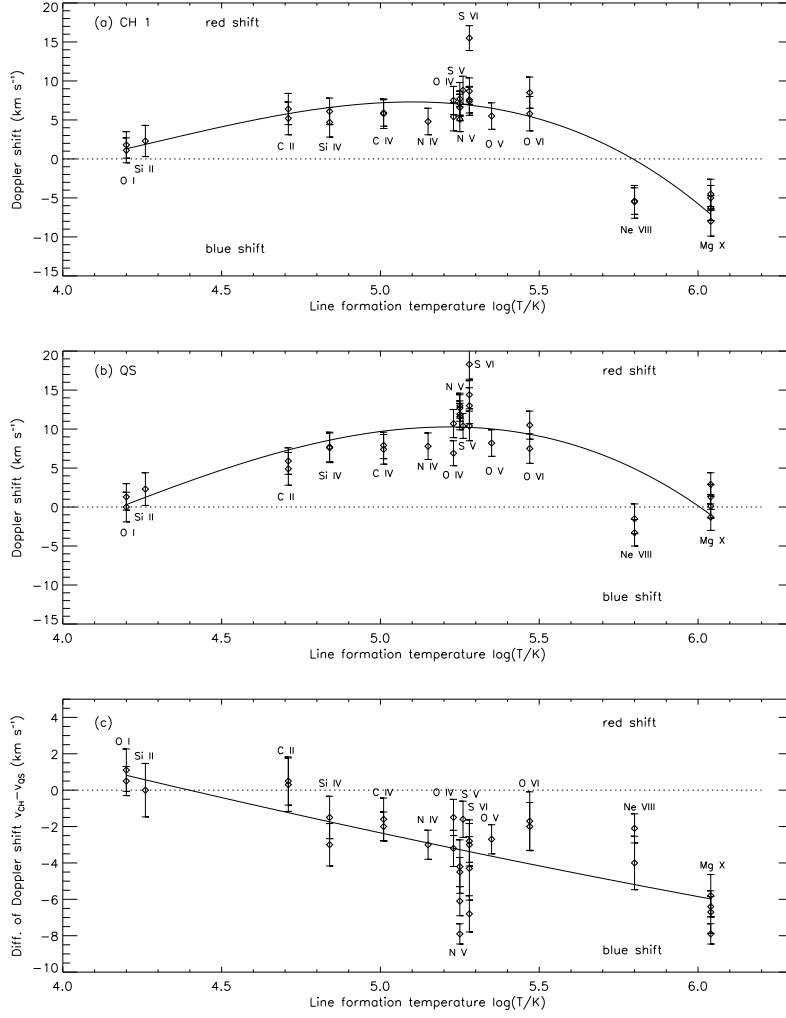


**Figure 2.** Average Doppler shifts of several spectral lines with different formation temperatures (Xia, Marsch, and Wilhelm, 2004). (a) A coronal hole region. (b) A quiet-Sun region. (c) Difference of the Doppler shifts between the coronal hole and quiet-Sun regions. Reproduced with permission from *Astronomy & Astrophysics*, © ESO.

this line. The same rest wavelength was also found independently by Peter and Judge (1999). Using this rest wavelength, the Ne VIII 770 Å line was found to be blueshifted by  $\approx 2 \text{ km s}^{-1}$  on average (e.g. Peter and Judge, 1999; Teriaca, Banerjee, and Doyle, 1999; Xia, Marsch, and Wilhelm, 2004). Dopplergrams of Ne VIII 770 Å obtained through raster scans revealed very prominent blue shifts at junctions of multiple adjacent network structures (e.g. Hassler et al., 1999; Dammasch et al., 1999; Aiouaz, 2008; Tian et al., 2008). These localized blue shifts could reach  $5\text{--}10 \text{ km s}^{-1}$  (Figure 1). They generally correspond to the legs of magnetic loops reconstructed through force-free magnetic-field extrap-

ulations, indicating mass supply to the corona along flux tubes rooted in the chromospheric network (Tian et al., 2009). Using the Doppler shift of Ne VIII as a proxy for the plasma bulk flow (i.e. the proton flow), these authors also found an anti-correlation between the flux tube expansion factor and mass flux.

## 2.2. Coronal Holes

A similar dependence of Doppler shift on formation temperature has also been found in coronal holes. From Figure 1 we can see that the C IV 1548 Å line is also predominantly redshifted in coronal holes. However, a distinct difference can be found between the C IV Dopplergrams in the quiet Sun and coronal holes, i.e. there are more pixels with blue shifts in a coronal hole than in an equally-sized quiet-Sun region (Dammasch et al., 1999). Figure 1 shows that Ne VIII 770 Å is blueshifted almost everywhere in a polar coronal hole, which is also distinctly different from the localized blue shifts of Ne VIII in the quiet Sun. The prevalence of blue shifts has been found in both polar and equatorial coronal holes (Hassler et al., 1999; Wilhelm et al., 2000; Xia, Marsch, and Curdt, 2003; Tu et al., 2005a; Aiouaz, Peter, and Lemaire, 2005). These prevalent blue shifts have been observed in not only the Ne VIII 770 Å line, but also in higher-temperature coronal lines such as Fe X 184.54 Å and Fe XII 195.12 Å (Tian et al., 2010, 2011a; Fu et al., 2014). As a result, the spatially averaged Doppler shift in coronal holes is generally blueshifted relative to that in the quiet Sun for spectral lines formed in a wide range of temperatures in the TR and lower corona (Xia, Marsch, and Wilhelm, 2004; Raju, 2009). Using SUMER observations, Xia, Marsch, and Wilhelm (2004) found that the difference increases with temperature from about  $\log T = 4.4$  to  $\log T = 6.0$  (Figure 2). With EIS observations of more coronal lines, Tian et al. (2010) found that this difference continues to increase with temperature until at least  $\log T \approx 6.3$ .

The net blue shifts of spectral lines with a formation temperature higher than  $\approx 5 \times 10^5$  K in coronal holes are generally believed to be signatures of the nascent fast solar wind (e.g. Hassler et al., 1999; Wilhelm et al., 2000; Xia, Marsch, and Curdt, 2003). The three-dimensional (3D) coronal magnetic field could be reconstructed from a measured photospheric magnetogram through a potential or force-free field extrapolation, and it can thus be used to correlate with the plasma flow pattern (Wiegmann, Xia, and Marsch, 2005). Using a similar method, Tu et al. (2005a) identified many funnel-like magnetic-flux tubes rooted in the chromospheric network of a coronal-hole region, and found that patches of large Ne VIII blue shift are closely associated with these funnels, suggesting that the nascent fast solar-wind flows outward along these expanding magnetic funnels (Figure 3). They calculated the correlation coefficient between maps of the Ne VIII blue shift and magnetic-field inclination at each height, and they found a maximum correlation at a height of  $\approx 20$  Mm above the photosphere. This height could be regarded as a rough estimate of the real formation height of Ne VIII 770 Å, because the motion of the emitting ions is expected to be largely guided and controlled by the shape of the expanding funnels at the line-emission height in the low- $\beta$  environment.

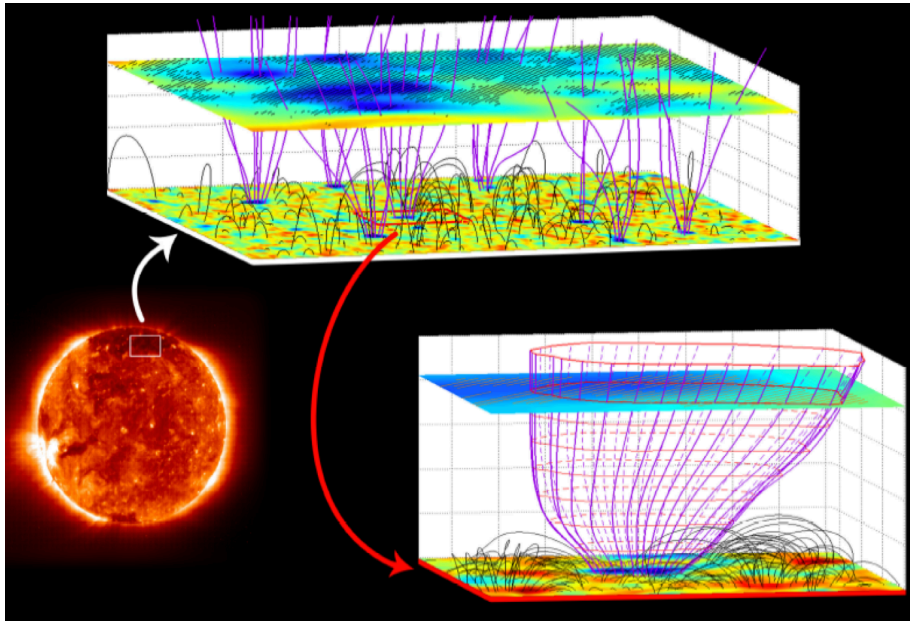


**Figure 3.** Solar wind origin from funnel-like magnetic structures (Tu et al., 2005b). Lower left: a full-disk coronal image. Top: reconstructed 3D magnetic-field structures in the white rectangular region. The black and purple lines represent closed- and open-field lines, respectively. A photospheric magnetogram (radial component, blue and red colors indicate different polarities) is shown at the bottom. The higher plane shows the magnetogram at 20 Mm, with the hatched region indicating largest blue shifts ( $\geq 7 \text{ km s}^{-1}$ ) of Ne VIII 770 Å. Lower right: zoomed-in view of the region indicated by the red rectangle.

It is worth mentioning that apparent jet-like features at coronal temperatures have been frequently reported in coronal holes (e.g. Cirtain et al., 2007; Ni et al., 2020; Shen, 2021). Many of these jets are associated with coronal bright points. In addition, Young (2015) found a new type of jet that is visible in the spectroscopic data but shows no clear signature in the imaging data. They are rooted in bright points and have speeds reaching  $\approx 100 \text{ km s}^{-1}$ . These sporadic jets are possibly not the dominant cause of the net blue shifts.

### 2.3. Mass Cycle between the Chromosphere and Corona

The observed temperature dependence of the Doppler shift is still not well understood. Tu et al. (2005a) and He, Tu, and Marsch (2008) interpreted the blue and red shifts in coronal holes as the bidirectional flows generated by magnetic reconnection between the open-field lines in coronal funnels and adjacent low-lying loops. A similar continuous reconnection between legs of large coronal loops (strong network field) and low-lying loops (weak field in internetwork regions) might also exist in the quiet Sun, resulting in bidirectional flows that account for the blue shifts of hotter lines and red shifts of cooler lines (Aiouaz, 2008).

An alternative interpretation, which has received much more attention in the community, considers the mass-circulation process in the solar atmosphere.

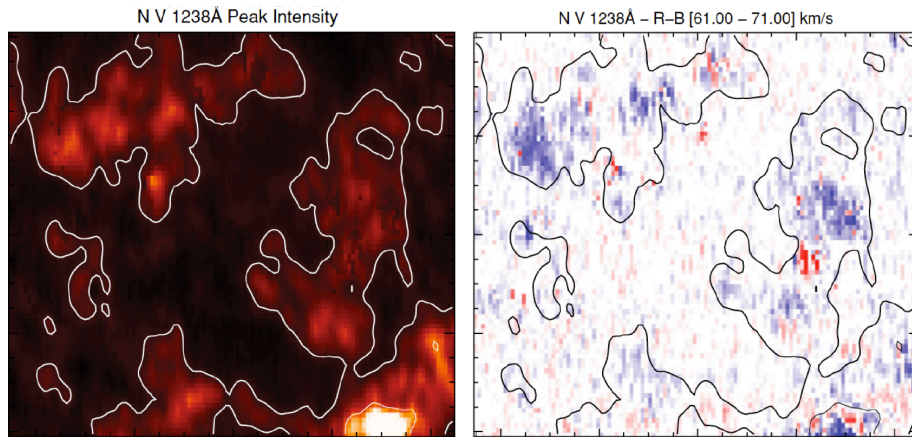


**Figure 4.** Images of N V 1238 Å intensity and profile asymmetry (McIntosh and De Pontieu, 2009a). Blue and red colors in the asymmetry image indicate enhancements of the 61–71 km s<sup>-1</sup> (from line centroid) spectral range at the blue and red wings, respectively. The contours outline regions of strong intensity. The FOV of each image is 90''×80''. Reproduced by permission of the AAS.

Although spectral lines with different formation temperatures show different signs of net Doppler shifts, a careful examination of the TR spectral-line profiles observed by SUMER and IRIS in network regions suggests that the spectral profiles are often enhanced at the blue wing (Figure 4). The blue-wing enhancement or blueward asymmetry has been found to occur intermittently, suggesting the presence of episodic weak ( $\approx 5\%$  of the line core intensity) high-speed ( $\approx 50\text{--}120$  km s<sup>-1</sup>) upflows (McIntosh and De Pontieu, 2009a; De Pontieu et al., 2009; Chen et al., 2019b). SUMER observations show that the weak blueward asymmetry can be identified from spectral lines formed in a wide range of temperatures, at least from  $\approx 7 \times 10^4$  K to  $\approx 7 \times 10^5$  K (McIntosh and De Pontieu, 2009a). These authors interpreted the observed emission of the TR and lower corona as a mixture of emission from rapid injection of episodically heated plasma to the corona and slow cooling of the previously heated plasma. They conjectured that the high-speed plasma ejections could be heating signatures of the high-speed spicules observed in the chromosphere (De Pontieu et al., 2007). With simultaneous imaging and spectroscopic observations of the TR, Tian et al. (2014b) discovered prevalent high-speed intermittent jets with a temperature of at least  $\approx 10^5$  K, and they demonstrated that the blueward asymmetry of the Si IV 1393 Å line is indeed caused by the superposition of these fast TR jets on the TR background. Some of these TR jets have been found to be heating signatures of chromospheric spicules (Pereira et al., 2014; Rouppe van der Voort et al., 2015), whereas others might be classified as the smallest jetlets (Raouafi and Stenborg, 2014; Panesar et al., 2018). Following the idea that the mass-cycling process is responsible for the observed TR emission, Wang et al. (2013) considered each spectral-line profile as a sum of three components: a high-speed heated upflow generated in the chromosphere, a nearly static background, and a slow cooling downflow. Their detailed investigation suggests that the varying

relative contributions of the three components at different temperatures might be responsible for the observed temperature dependence of Doppler shift. The more or less steady behavior of the observed Doppler shifts suggests that such a mass-cycling process should occur continuously.

Numerical simulations have also been performed to understand the temperature dependence of Doppler shift. Gudiksen and Nordlund (2005) developed a 3D magnetohydrodynamic (MHD) model of the solar corona, where the coronal heating is due to the magnetic braiding induced by field line footpoint motions in the photosphere. Peter, Gudiksen, and Nordlund (2004) and Peter, Gudiksen, and Nordlund (2006) took this model and synthesized spectra of several TR and coronal lines. They found that this model can reproduce the observed temperature dependence of the TR red shift, implying that the well-known TR red shifts are caused by the flows induced by heating through braiding of magnetic-field lines. However, the model predicted a net red shift for the Ne VIII 770 Å and Mg X 625 Å lines that are formed in the upper TR and lower corona, which is inconsistent with SUMER observations but might be due to the relatively low height of the upper boundary. Using 3D MHD models spanning the upper convection zone to 15 Mm above the photosphere, Hansteen et al. (2010) found that rapid intermittent heating of the plasma from the upper chromosphere to coronal temperatures naturally produces net red shifts for most TR lines and small blue shifts of spectral lines formed above a temperature of  $\approx 5 \times 10^5$  K, roughly consistent with SUMER and EIS observations. These episodic heating events are accompanied by the generation of intermittent high-speed multi-thermal upflows, which may be related to the fast chromospheric spicules (De Pontieu et al., 2007), TR network jets (Tian et al., 2014b), and high-speed upflows inferred from the blueward asymmetries of TR lines observed by SUMER (McIntosh and De Pontieu, 2009a). From high-resolution measurements of the photospheric magnetic field, Samanta et al. (2019) demonstrated that intermittent magnetic reconnection between the strong network field and the newly emerged, weak, small-scale internetwork field is likely responsible for the generation of at least some of these upflowing materials.

### 3. Upflows from Active-Region Boundaries

The dominant emission structures in the upper solar atmosphere of ARs are large-scale loops that outline the strong magnetic field. Prominent red shifts of spectral lines formed in the TR are commonly observed in these coronal loops, particularly at the loop legs (e.g. Winebarger et al., 2002; Marsch, Wiegelmann, and Xia, 2004; Dammasch et al., 2008; Marsch et al., 2008; Del Zanna, 2008). Different from the TR red shifts observed in the network lanes of quiet-Sun regions and coronal holes, these red shifts are also present in coronal lines with a formation temperature as high as  $\approx 10^{6.2}$  K (Del Zanna, 2008). The magnitude of these red shifts could reach  $\approx 30 \text{ km s}^{-1}$ , two to three times higher than in the quiet Sun and coronal holes. Despite these differences, the origin of these red shifts is likely to be similar to that in the quiet Sun and coronal holes (e.g. Dammasch et al., 2008).



At the boundaries of many ARs, the coronal emission is normally weaker than in the AR cores. With SOHO/SUMER observations, Marsch, Wiegmann, and Xia (2004) found signatures of upflows in the Ne VIII 770 Å line, which is formed in the upper TR or lower corona, at the boundaries of ARs. With *Hinode*/EIS observations, coronal spectral lines such as Fe XII 195.12 Å and Fe XIII 202.04 Å are often found to be blueshifted (e.g. Harra et al., 2008) (Figure 5). This is one of the major discoveries of EIS. Early results about these blueshifts have been summarized by Harra (2012), and there has also been a short summary of studies connecting the upflows to the solar wind using EIS observations (*Hinode* Review Team et al., 2019). In this section we provide an updated and more extended review of past investigations on these upflows.

### 3.1. Velocity Measurements

These blue shifts appear to be quasi-steady, i.e. they generally last for at least a few days (e.g. Baker et al., 2009; Bryans, Young, and Doschek, 2010; Tian et al., 2012b). A single Gaussian fit (SGF) to the observed coronal line profiles often leads to a blue shift of  $\approx 10-50 \text{ km s}^{-1}$  (e.g. Harra et al., 2008; Marsch et al., 2008; Doschek et al., 2008; Srivastava et al., 2014). These blue shifts are associated with enhanced line broadenings (or nonthermal velocities), and there is a positive correlation between them (e.g. Doschek et al., 2008). From magnetic-field extrapolations, these upflows appear to be guided by the legs of large-scale magnetic loops or open magnetic-field structures at AR boundaries (e.g. Marsch, Wiegmann, and Xia, 2004; Harra et al., 2008; Marsch et al., 2008; Baker et al., 2009). These structures expand rapidly with height, often appearing as fan-like structures. The upflows are normally more obvious towards the footpoints of the fans, but are not always associated with them (Warren et al., 2011). They are, however, sometimes very prominent in low-emission regions at the peripheries of AR cores or between the cores and fans (e.g. McIntosh et al., 2012; Scott, Martens, and Tarr, 2013).

Démoulin et al. (2013) and Baker et al. (2017) tracked several ARs as they crossed the solar disk. By applying a simple model of stationary upflow to the observed ARs, they found that the long-term evolution of the persistent upflows is consistent with the scenario of steady upflows projected onto the line of sight (LOS). They found no obvious dependence of the de-projected upflow velocity on the AR age. They were also able to determine the inclination angles of the magnetic-field lines that guide the upflows. Baker et al. (2017) found that the inclination angles are typically in the range of  $[0^\circ, 40^\circ]$  and  $[-30^\circ, 30^\circ]$  relative to the local vertical direction for the trailing and leading polarities, respectively. These angles are roughly consistent with those inferred from magnetic-field extrapolations. The upflow velocities show no obvious difference between the trailing and leading polarities and do not depend on the underlying photospheric magnetic-field strength. They also found that transient coronal events such as CMEs, jets, and flares could lead to a variation of the upflow velocities on different time scales. However, these transient changes normally do not affect the quasi-steady behavior of the upflows.

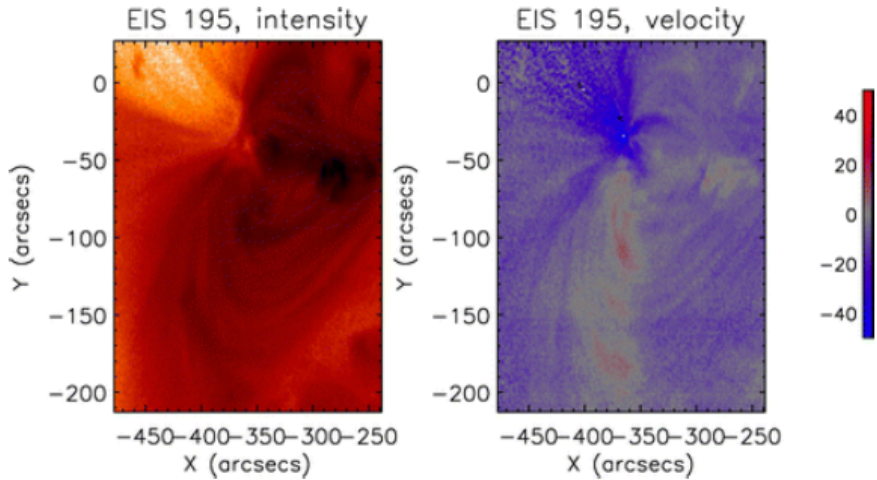


**Figure 5.** Intensity image (shown with a reversed color table) and Dopplergram of the Fe XII 195.12 Å line obtained during a raster scan of *Hinode*/EIS (Harra et al., 2008). Reproduced by permission of the AAS.

These upflows first appear during the phase of flux emergence and generally persist during the whole lifetimes of ARs. Harra et al. (2010) performed a detailed investigation of an emerging AR, and they witnessed the formation of these upflows. As the AR expands, they observed a ring of blue shifts in coronal spectral lines around the edge of the emerging AR. The upflows clearly intensify as more magnetic flux emerges. In a subsequent study, Harra et al. (2017) tracked the evolution of a decaying AR during three solar rotations, and they found a larger area occupied by upflows and slightly higher upflow speeds as the AR evolves. Zangrilli and Poletto (2016) extended investigations of AR upflows on the solar disk to the off-limb corona utilizing observations from the *Ultraviolet Coronagraph Spectrometer* (UVCS: Kohl et al., 1995) onboard SOHO. Their findings demonstrated that upflows persist over the lifetime of an AR spanning over four solar rotations.

Through an examination of the coronal line profiles at AR boundaries, Hara et al. (2008) found that the profiles are generally asymmetric, with a weak yet noticeable enhancement at the blue wings. These blueward asymmetries suggest the presence of unresolved high-speed upflows. Later, detailed analyses of these line profiles suggest that the coronal emission consists of at least two components: a primary component accounting for the nearly stationary background emission and a secondary component associated with high-speed upflows (e.g. Tian et al., 2011b; Brooks and Warren, 2012). Figure 6 shows examples of such line profiles, which also indicate a temperature dependence of the high-speed component. Several methods have been introduced to separate the two components and characterize the weak high-speed component, including the technique of double-Gaussian fit (Peter, 2010; Bryans, Young, and Doschek, 2010; Brooks

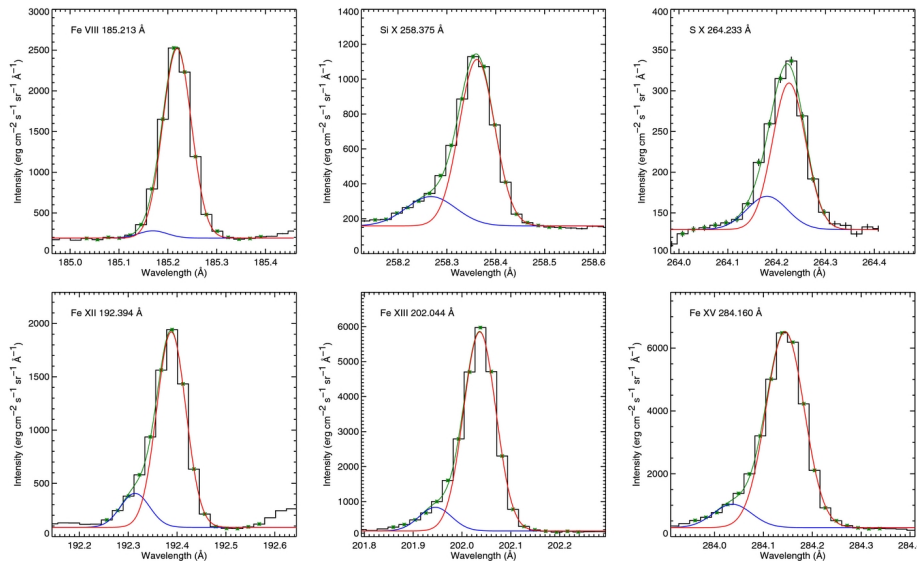


**Figure 6.** Double-Gaussian fits to several line profiles observed at an AR boundary (Brooks and Warren, 2012). The histograms represent the observed line profiles. In each panel, the primary and secondary components are shown as the red and blue curves, respectively. The green curve represents the total of the two components. Reproduced by permission of the AAS.

and Warren, 2012; Doschek, 2012; Kitagawa and Yokoyama, 2015), red–blue (RB) asymmetry analysis (De Pontieu et al., 2009; De Pontieu and McIntosh, 2010; Martínez-Sykora et al., 2011; Tian et al., 2011b; Tian, McIntosh, and De Pontieu, 2011) and RB-guided double-Gaussian fit (De Pontieu and McIntosh, 2010; Tian et al., 2011b). Application of these methods to the observed coronal spectral-line profiles at AR boundaries mostly yielded speeds on the order of  $\approx 100 \text{ km s}^{-1}$ , often in the range of  $50 - 150 \text{ km s}^{-1}$ , for these high-speed upflows. Occasionally the velocity may reach  $\approx 200 \text{ km s}^{-1}$ . The primary component is often also blueshifted, but by only  $\approx 10 \text{ km s}^{-1}$ . The intensity ratio of the two components is mostly less than 15%, although at some locations it could reach more than 30%. The widths of the two components are often comparable, which has also been confirmed through a comparison with analysis of artificial profiles (Tian et al., 2011b). Since an observed spectral-line profile is the superposition of the two components, an enhanced line broadening and a moderate blue shift ( $\approx 10 - 50 \text{ km s}^{-1}$ ) are expected if a SGF is applied. This superposition also explains the observed positive correlation of the blueward asymmetry with the blue shift and line broadening determined from a SGF (Tian et al., 2011b). It is worth mentioning that a blue-wing enhancement could in principle result from the superposition of multiple (more than two) emission components, each slightly Doppler-shifted with respect to each other (Doschek, 2012). This scenario might explain some of the AR upflows but is not very likely for all of them, because at some locations the blue-wing enhancement is so strong and far from the line core that a multiple-component scenario is really not consistent with the observed line profiles. In addition, speeds of the counterparts of these upflows in coronal image

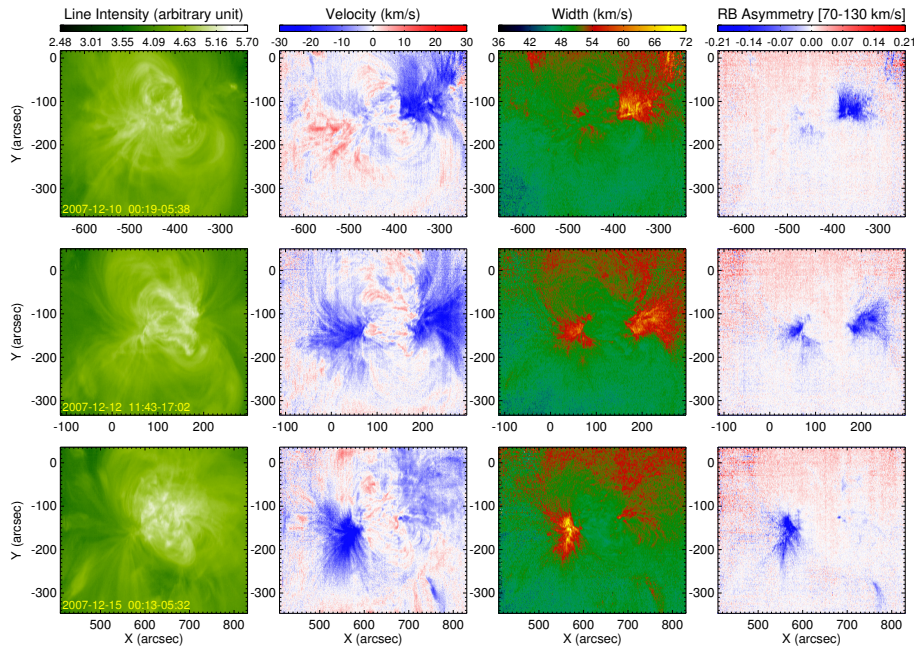


**Figure 7.** Maps of the SGF parameters and profile asymmetry in the velocity interval of  $70\text{--}130\text{ km s}^{-1}$  (Tian et al., 2012b). The first, second, and third rows correspond to observations of the same AR when it is located near the east limb, disk center, and west limb, respectively. Reproduced by permission of the AAS.

sequences (see Section 3.2) can often be unambiguously measured and they do not show a continuous distribution.

Although the blueward asymmetries are weak, they are definitely not caused by random noise or blends by other spectral lines. Tian et al. (2012b) have demonstrated this by tracking an AR as it rotates from the east limb to the disk center and then to the west limb. From Figure 7 we see a clear center-to-limb variation of the line parameters. Here the RB asymmetry is defined as the difference of the two wing intensities integrated over the velocity interval of  $70\text{--}130\text{ km s}^{-1}$  divided by the peak intensity. When the AR is located near the disk center on 12 December 2007, we see prominent blue shifts, large line broadenings, and blueward asymmetries at both boundaries. As the AR rotates to the west limb on 15 December 2007, the profile asymmetries disappear at the western boundary. This phenomenon can be understood if we consider the scenario of a high-speed field-aligned upflow superimposed on a nearly static coronal background. When the AR is close to the west limb, the magnetic-field lines at the western boundary are roughly perpendicular to the LOS so that the projected speed of the field-aligned flow on the LOS direction is very small. This leads to a greatly reduced blueward asymmetry as well as a reduced Doppler shift and line broadening. Similarly, when the AR is located near the east limb on 10 December 2007, the blue shift, line broadening, and blueward asymmetry are all reduced at the eastern boundary because the field lines are roughly perpendicular to the LOS there.

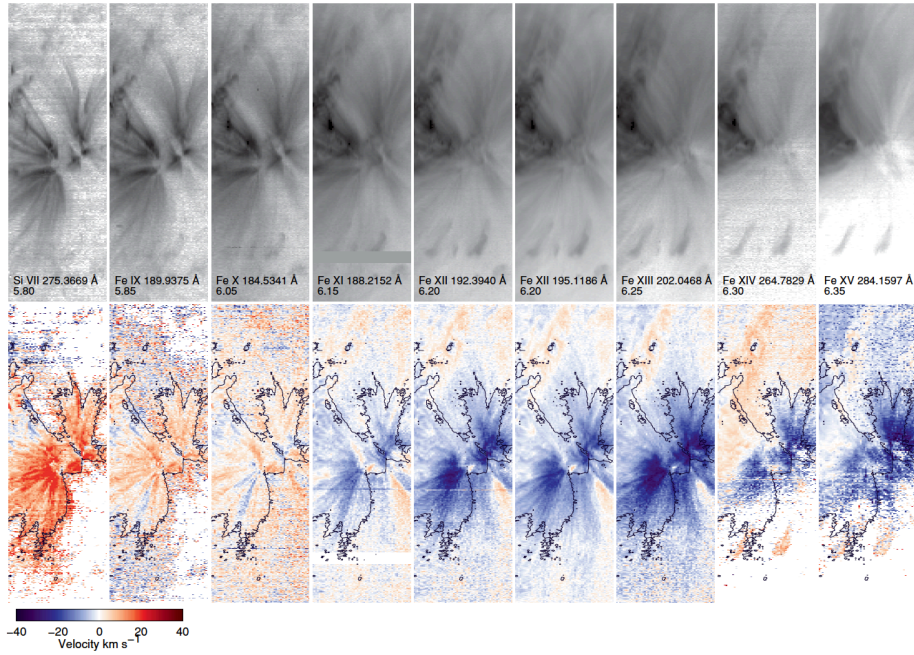


**Figure 8.** Intensity images (shown with a reversed color table) and Dopplergrams of several emission lines at an AR boundary (Warren et al., 2011). Contours of the Si VII 275.35 Å intensity is overlaid on the Dopplergrams. The FOV of each image is about  $180'' \times 512''$ . Reproduced by permission of the AAS.

There is a clear dependence of the SGF velocity on the line-formation temperature at AR boundaries. Del Zanna (2008) found that the SGF blue shift increases from only a few  $\text{km s}^{-1}$  at  $10^{5.8}$  K to  $\approx 30 \text{ km s}^{-1}$  at  $10^{6.3}$  K at an AR boundary. Tripathi et al. (2009) analyzed the EIS data at another AR boundary. They found an average red shift of a few  $\text{km s}^{-1}$  for the Si VII 275.35 Å line formed at  $\log T \approx 5.8$ , and an increase of the average blue shift from  $\approx 2 \text{ km s}^{-1}$  at  $10^{6.0}$  K to  $\approx 10 \text{ km s}^{-1}$  at  $10^{6.3}$  K. Actually, at AR boundaries both downflows and upflows could exist in the TR line Si VII 275.35 Å. McIntosh et al. (2012) found that this line is redshifted at the fan-like structure of an AR and blueshifted in a dark region between the fan and the AR core. If we only consider fan-like structures, a clear trend from red shifts to blue shifts is normally observed in the temperature range of  $\log T = 5.8$  to 6.3 (Figure 8). The transition from red shifts to blue shifts occurs at a temperature of  $\log T \approx 6.0$ , meaning that spectral lines formed at typical coronal temperatures and TR temperatures are predominantly blueshifted and redshifted, respectively. We note, however, that there are cases where the morphology of the fans and upflows is different, and there is no fan emission at low temperatures beneath the upflows (Warren et al., 2011).

By examining the EIS line-profile asymmetries and slot images, Ugarte-Urra and Warren (2011) have attempted to understand the different Doppler shift patterns of coronal lines and TR lines. They identified clear outward-propagating disturbances with speeds of  $40\text{--}130 \text{ km s}^{-1}$  from the Fe XII 195.12 Å image se-

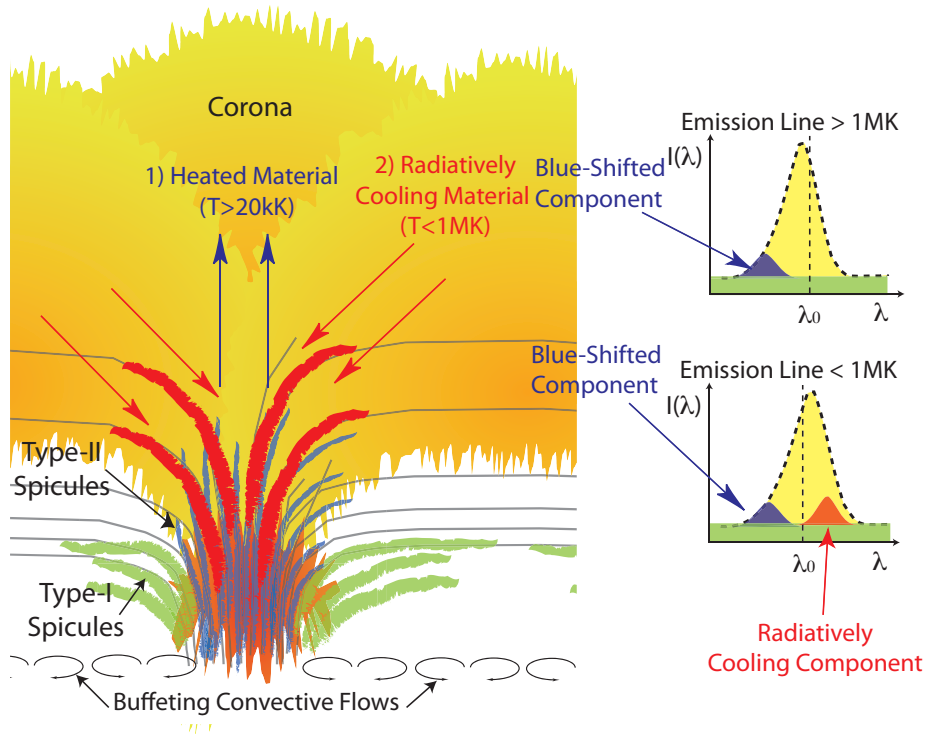


**Figure 9.** A cartoon showing the mass cycling between the chromosphere and corona (McIntosh et al., 2012). Reproduced by permission of the AAS.

quence, consistent with the quasi-periodic blue-wing enhancements in the Fe XII line profiles. From the Si VII 275.35 Å slot images, they could not identify any obvious signature of outward-propagating features. Instead, they identified downward-propagating features with speeds of 15–20 km s<sup>-1</sup>, which are comparable to the magnitude of red shifts at the locations of fans. From imaging observations of AIA, Kamio et al. (2011) and McIntosh et al. (2012) have also identified quasi-periodic fast ( $\approx 100$  km s<sup>-1</sup>) outward-propagating disturbances in the hot 193 Å channel and sporadic slow ( $\approx 15$  km s<sup>-1</sup>) downflows in cool channels such as 131 Å. McIntosh et al. (2012) also found a mixture of upflows and downflows from the 171 Å images, indicating that the dominant flow changes its direction around a temperature of  $\approx 1$  MK.

These observations imply a mass-cycling process between the chromosphere and corona (Figure 9). As McIntosh et al. (2012) suggested, local chromospheric materials may be impulsively heated, producing high-speed upflows with typical TR and coronal temperatures. As these upflows experience significant radiative cooling, the previously heated and injected plasma will slowly drain to the chromosphere. These downflows may have a typical temperature of the TR plasma. EIS observations have shown that TR lines such as Si VII 275.35 Å also reveal blueward asymmetries (Tian et al., 2011b; McIntosh et al., 2012). However, the velocity of the secondary component inferred from Si VII line profiles appears

to be smaller than that inferred from the simultaneously observed coronal line profiles, which is likely due to the fact that TR line profiles are complicated by downflows. Unlike the two-component coronal line profiles, a TR line profile likely consists of three components: a fast upflow component generated through chromospheric heating, a slow cooling downflow component, and a TR background component. The downflows have a much lower speed and possibly stronger emission compared to the upflows, which would result in net red shifts of the TR lines when a SGF is performed. So similar to the quiet Sun and coronal holes, the temperature dependence of the SGF Doppler shift at AR boundaries is probably caused by the relative contributions of the different components at different temperatures. A similar scenario of mass cycling or circulation has also been proposed by Marsch et al. (2008) and Young, O’Dwyer, and Mason (2012).

Sometimes the red-shifted downflows on the fan loops appear to be spatially uncorrelated with the blue-shifted upflows (as in one of the examples in Warren et al., 2011). In these cases the mass-circulation picture might still be relevant if the upflows are connected to a distant AR (as in Boutry et al., 2012), i.e. the red shifts on the fans of the distant AR might be signatures of the circulation. In such cases the morphology of the fan loops and upflows is similar because of the general topology of the magnetic field at the active-region boundary (Baker et al., 2009).

### 3.2. Waves or Flows

From EUV and X-ray imaging observations, we often find quasi-periodic upward propagating disturbances (PDs) along the fan-like structures at AR boundaries (e.g. De Moortel, Ireland, and Walsh, 2000; Sakao et al., 2007; Yuan and Nakariakov, 2012). These PDs have a propagation speed of  $\approx 50 - 200 \text{ km s}^{-1}$ , and they often recur at a time scale of 3–15 minutes. These PDs were widely interpreted as slow-mode magnetoacoustic waves propagating along the fans, mainly because the speed is comparable to the coronal sound speed and there is a correlation between the intensity and velocity perturbations (de Moortel, 2009; Wang et al., 2009; Wang, Ofman, and Davila, 2009; Nishizuka and Hara, 2011).

The aforementioned blue shifts and these PDs are often found at the same locations, indicating that they are closely related to each other. Based on this coincidence, the PDs have been suggested to be plasma upflows (Sakao et al., 2007; Harra et al., 2008). However, there appear to be some distinct differences between them. First, around the year 2008, it was unclear why the blue shifts are only  $\approx 10 - 50 \text{ km s}^{-1}$ , which are significantly lower than the speeds of PDs. A projection effect has been proposed to explain the apparent discrepancy between the LOS velocities of the blueshifts and the plane-of-sky (POS) velocities of the PDs. However, the blue shifts seldom exceed  $50 \text{ km s}^{-1}$ , regardless of AR location on the solar disk. Second, the PDs are clearly quasi-periodic. However, it was unclear whether the blue shifts showed a quasi-periodic variation around 2008.

These discrepancies disappear if we compare the PDs with the high-speed secondary components of coronal line profiles. From a coordinated observation with XRT and EIS onboard *Hinode*, Tian, McIntosh, and De Pontieu (2011) found a clear correspondence between the fluctuations of the X-ray intensity

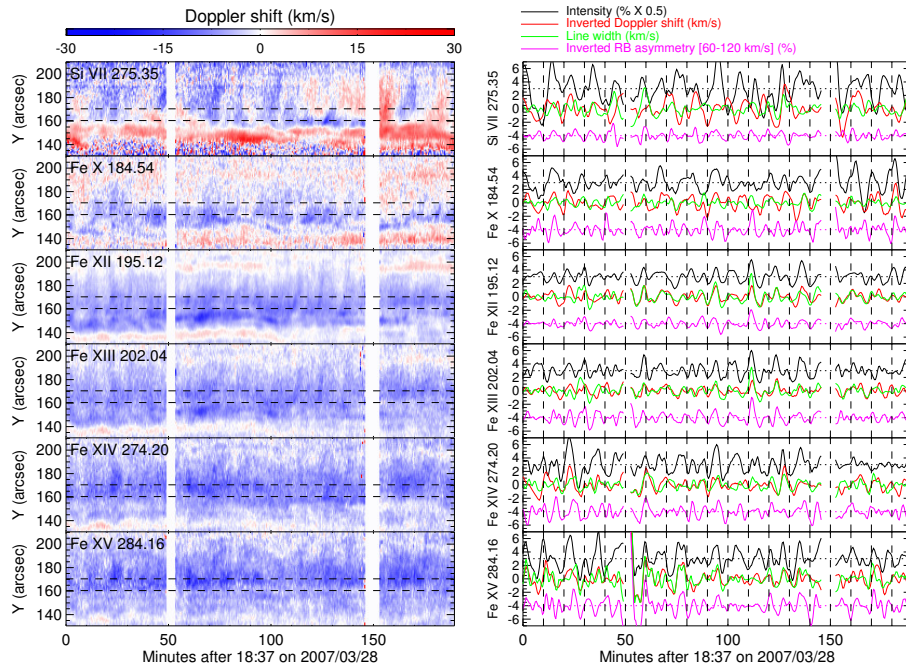


**Figure 10.** Quasi-periodic variation of the AR upflows (Tian et al., 2012a). Left: Temporal evolution of the Doppler shift of several emission lines. Right: Curves with different colors represent the temporal changes of the line intensity, Doppler shift, line width, and profile asymmetry (RB asymmetry) averaged within the region between the two dashed lines in each of the left panels. For a clearer illustration, the intensity and asymmetry curves are offset by 3 and -4, respectively. Reproduced by permission of the AAS.

and the blueward asymmetries of coronal spectral lines, suggesting that the PDs observed in XRT images are closely related to the secondary components. Through joint observations of SDO/AIA and *Hinode*/EIS, Tian et al. (2011b) demonstrated that the velocity distributions and relative intensities are both remarkably similar for the simultaneously observed PDs and secondary components. In addition, with sit-and-stare observations of EIS, De Pontieu and McIntosh (2010) and Tian, McIntosh, and De Pontieu (2011) noticed that the blue shifts and blueward asymmetries often show quasi-periodic variations. A following statistical study by Tian et al. (2012a) demonstrated that this behavior is quite common, and that the recurring time scale is similar to that of PDs. So it appears that the PDs are related to the high-speed secondary components.

Detailed analyses suggest that the blueward asymmetry as well as the intensity, blue shift and line width derived from a SGF all reveal correlated quasi-periodic variations. Figure 10 shows an example. The quasi-periodic enhancement of blue shift is clearly seen from the space-time diagrams. For the spectral lines formed at typical coronal temperatures of  $\log T = 6.0 - 6.3$  (Fe x 184.54 Å, Fe XII 195.12 Å, Fe XIII 202.04 Å, Fe XIV 274.20 Å, and Fe XV 284.16 Å), we can see correlated changes of all these line parameters. Such correlated changes can be explained by a scenario of recurring or quasi-periodically enhanced upflows (De Pontieu and McIntosh, 2010; Tian, McIntosh, and De Pontieu, 2011; Tian



et al., 2012a). On occasions when there is only the nearly stationary background-emission component and no upflow, the Doppler shift is zero and the spectral profile is symmetric. While when a high-speed upflow component coexists with the background component, a SGF to the total emission profile will lead to an increase in the line intensity and line width. In the meantime, the line profile reveals an enhancement in the blue wing and a SGF gives a small blue shift. This scenario naturally explains the in-phase variations of all line parameters, which appears to favor the interpretation of intermittent plasma jets for the PDs. If this new interpretation is correct, previous diagnostics of the coronal plasma based on the wave interpretation of PDs would be significantly impacted.

However, there is also observational evidence supporting the slow-wave interpretation. For instance, Verwichte et al. (2010) considered a scenario of propagating slow waves with a quasi-static background plasma component in the LOS. They were able to reproduce a blueward asymmetry in the line profiles, and a correlation of the blueward asymmetry with the line intensity and blue shift. They concluded that the slow-wave interpretation is still valid for the PDs. However, their model predicted a double frequency (or half period) in the line width that is not seen in EIS observations. There are also a couple of studies reporting a temperature-dependent PD velocity (Krishna Prasad, Banerjee, and Singh, 2012; Uritsky et al., 2013), which is a characteristic of slow-mode magneto-acoustic waves. However, several other studies did not reveal any obvious temperature dependence (Tian et al., 2011b; Sharma et al., 2020). A statistical study by Kiddie et al. (2012) showed that the temperature dependency appears to be clear only for PDs rooted in sunspots.

After several years of debate, there is now a consensus that both waves and flows exist at AR boundaries. For example, recent IRIS and AIA observations have revealed signs of magneto-acoustic shock waves and jet-like flows, both of which appear to show a correspondence to the PDs (Bryans et al., 2016). As shown in Figure 11, the quasi-periodic sawtooth-like patterns in the Mg II h 1403 Å spectral profiles (evidence of magnetoacoustic shock waves, e.g. Rouppe van der Voort et al., 2003; Tian et al., 2014a; Skogsrud, Rouppe van der Voort, and De Pontieu, 2016), the Si IV blue shifts (signs of jet-like flows) and the PDs in 171 Å appear to be correlated. Thus both waves and flows may contribute to the signals of PDs. From EIS observations, the enhanced line width and blueward asymmetry are most obvious at the lower parts of fan structures, and they become absent at higher parts. This observational fact might be explained by a LOS projection effect or lower signals at larger heights. However, it could also be explained as due to the dominance of slow-mode waves away from the footpoint regions. Indeed, Nishizuka and Hara (2011) found an in-phase variation of the coronal-line intensity and Doppler shift at larger heights, which was interpreted as an evidence of slow-mode waves. They also claimed that at lower heights fast upflows obviously exist and may be driven by heating events around the footpoints of loops.

Attempts have been made to understand the coexistence of waves and flows. For instance, Ofman, Wang, and Davila (2012) performed 3D MHD modeling of hot ( $\approx 6$  MK) AR loops, and found that impulsively and periodically driven

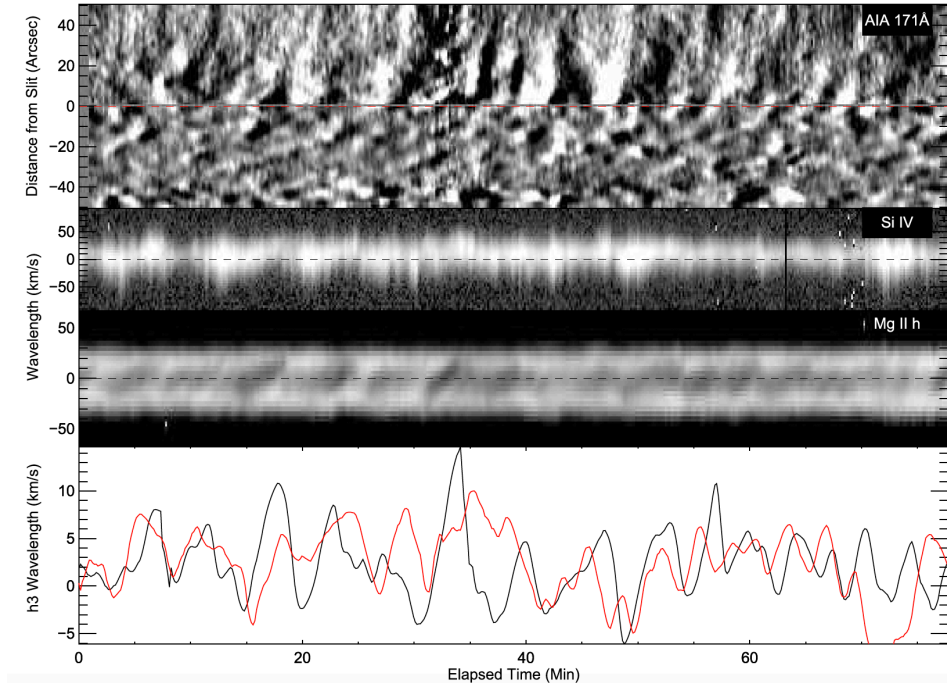


**Figure 11.** Contribution of PDs from both waves and flows (Bryans et al., 2016). Top panel: a space–time diagram of the AIA 171 Å running difference for a virtual slit along the leg of a fan loop. The red horizontal line indicates the IRIS slit location. Second and third panels: temporal evolution of the Si IV 1403 Å and Mg II h 1403 Å spectral line profiles. The black horizontal lines indicate the rest wavelengths of the two lines. Bottom panel: temporal evolution of the Mg II h3 Doppler shift (black) and the negative of the 171 Å intensity (normalized, red). Reproduced by permission of the AAS.

upflows can excite undamped slow-mode waves that propagate along the magnetic loops. Their simulations also generated slow-mode shock-like wave trains when the driving pulses have a large amplitude. In a subsequent numerical investigation, Wang, Ofman, and Davila (2013) expanded this model to warm loops ( $\approx 1$  MK) and found a similar result. They concluded that at lower heights both the flows and waves contribute to the PDs, while at larger heights the PDs are likely dominated by slow waves, as the flows decelerate during the upward propagation. However, these simulations assumed an isothermal plasma, the effect of which needs to be investigated in the future. In addition, the speeds of the upflow pulses in these simulations appear to be much smaller than the speeds of the secondary components inferred from EIS observations.

### 3.3. Generation Mechanisms

Baker et al. (2009) investigated the magnetic-field topology of an AR using a linear force-free field extrapolation method. From the reconstructed 3D coronal magnetic field, they identified quasi-separatrix layers (QSLs), which are locations

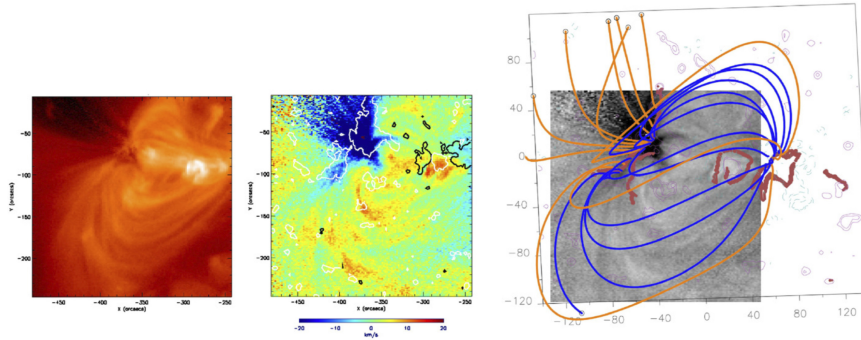


**Figure 12.** *Hinode*/EIS Fe XII 195 Å intensity (left) and Doppler velocity (middle) maps and photospheric traces of QSLs in thick red lines overlotted on a grayscale Dopplergram (right). MDI magnetic field isocontours of  $\pm 50$  G are shown in white/black (middle). Field lines with circles leave the computational box and are considered to be open field. Strong upflows (blue patches in the middle panel, or dark patches in the right panel) over the positive polarity are along open-field lines on the eastern edge of AR 10942 (Baker et al., 2009). The EIS images correspond to a FOV of about  $250'' \times 250''$ . Reproduced by permission of the AAS.

of strong gradients of magnetic connectivity. The strongest upflows appear to be located in the vicinity of QSL sections over areas of strong field. Based on this finding, the authors suggested that the upflows are driven by magnetic reconnection at QSLs between closed field lines at AR cores and open-field lines or large-scale externally connected loops from AR boundaries. Edwards et al. (2016) analyzed EIS data of seven ARs and found that the upflows generally do not correspond to high-reaching loops or open-field structures predicted by the global potential-field source-surface model, but they also found that the upflows often coincide with the footprints of separatrix surfaces that are associated with coronal null points. A good agreement between upflow regions and QSLs, either temporally or spatially or both, has also been found by Scott, Martens, and Tarr (2013), Démoulin et al. (2013), Mandrini et al. (2015), and Baker et al. (2017). Similarly, Démoulin et al. (2013) proposed that the upflows are driven by the upward pressure gradient after magnetic reconnection between the high-pressure AR loops and neighboring low-pressure loops. This scenario naturally explains the observational fact that stronger upflows are located closer to the AR cores. The steadiness of the upflows could be understood if we consider the scenario of successive reconnections, which leads to a superposition and thus averaging of flows with different velocities.

Del Zanna et al. (2011) studied two ARs and found a clear association of the upflows with metric radio noise storms and large-scale open separatrix field lines. Based on this connection, they proposed that the upflows are driven by interchange reconnection between magnetic loops in AR cores and adjacent open-field structures. In this scenario, continuous AR expansion leads to successive reconnection at coronal null points, which results in a strong pressure gradient that drives the temperature-dependent plasma upflows. Bradshaw, Aulanier, and Del Zanna (2011) numerically simulated this scenario and found the development

of a rarefaction wave in the post-reconnection region. Their forward calculation yielded a  $\approx 10\text{--}50\text{ km s}^{-1}$  blueshift and clear temperature dependence of the velocity magnitude, consistent with observational results based on a SGF (e.g. Del Zanna, 2008). On the other hand, a 3D data driven simulation of a similar mechanism by Galsgaard et al. (2015) failed to reproduce systematic upflows seen in EIS observations (Vanninathan et al., 2015). Instead, this model generated magneto-acoustic waves.

Besides magnetic reconnection, AR expansion has also been considered as a mechanism to drive the upflows. Murray et al. (2010) performed a 3D MHD simulation, and they found that an upward acceleration of the coronal plasma is achieved when an AR expands horizontally in a unipolar background-field environment. They have managed to reproduce upflow speeds up to  $45\text{ km s}^{-1}$ . Since AR expansion naturally leads to an intensification of the electric current at the interface between closed- and open-field structures, which favors the occurrence of magnetic reconnection, it is likely that reconnection and expansion both contribute to the generation of the AR upflows. This was demonstrated when upflow velocities are significantly enhanced on the side of an AR adjacent to the open field of a nearby coronal hole. The slow rise and expansion of a flux rope contained within the AR lead to stronger compression of the open field and the intensification of upflows hours before the flux rope erupts as a CME (Baker, van Driel-Gesztelyi, and Green, 2012). Using a similar approach, Harra et al. (2012) found that the upflows at the west and east sides of an emerging AR are dominated by reconnection jets and pressure-driven upflows, respectively.

Hara et al. (2008) conjectured that high-speed upflows inferred from the blueward asymmetries of coronal line profiles result from impulsive heating at the base of the corona, around the footpoints of AR loops. Based on an observed association of the episodic high-speed upflows with chromospheric activity, McIntosh and De Pontieu (2009b) suggested that these upflows represent discrete mass-injection events produced by episodic local heating of the chromosphere. A similar scenario was also proposed based on the similar velocity distributions of these high-speed coronal upflows and fast chromospheric spicules (De Pontieu et al., 2009). In limb observations, some chromospheric spicules appear to be heated to TR and coronal temperatures, exhibiting as upward propagating upflows in the AIA EUV passbands (De Pontieu et al., 2011). Based on these observations, these authors proposed that the high-speed coronal upflows are actually heating signatures during the upward propagation of spicule-like plasma jets that are possibly driven by magnetic reconnection (e.g. De Pontieu et al., 2009; Samanta et al., 2019; Chen et al., 2019b) or other processes such as amplified magnetic tension (Martínez-Sykora et al., 2017) in the chromosphere. They further pointed out that these episodic high-speed upflows generated at chromospheric heights play a key role in the mass and energy supply to the corona.

Although this scenario has received a lot of attention in the community, it has also been questioned by some studies. For instance, Klimchuk (2012) examined a scenario of spicule-supplied coronal plasma, which predicted a much larger blue-wing enhancement than observed. They concluded that spicules cannot provide

sufficient pre-heated plasma to fill the corona. Even if they did, additional heating would be needed to maintain the high temperature as the plasma expands upward and cools adiabatically. Klimchuk and Bradshaw (2014) and Bradshaw and Klimchuk (2015) performed one-dimensional hydrodynamic simulations for the idea of coronal heating by spicules, and they found that the synthesized coronal spectral-line profiles are distinctly different from the observed ones. They concluded that impulsive heating events in the chromosphere cannot explain the bulk of coronal heating, although they may be responsible for heating of the chromospheric spicules to TR temperatures. With EIS observations of multiple spectral lines formed at different temperatures, Tripathi and Klimchuk (2013) derived the emission-measure distribution for the secondary component, and they concluded that the emission measure is too small to support the proposal of coronal mass supply by chromospheric spicules. Using the density sensitive line pair Fe XIV 264.78 Å/274.20 Å, Patsourakos, Klimchuk, and Young (2014) found similar densities for the primary and secondary components at most pixels, which agrees with the prediction from a scenario of coronal mass supply through chromospheric evaporation driven by coronal nanoflares. Plasma composition measurements (see below) of the high-speed component by Brooks and Warren (2012) also support this scenario. This conclusion finds some support from observations by Vanninathan et al. (2015), who found no evidence of a spicule contribution to the AR upflows from simultaneous coronal and chromospheric observations, although their study was restricted to looking at asymmetries in the H $\alpha$  line profile, the formation of which is highly complex. In contrast, a recent study by Polito et al. (2020) has found clear evidence of a correlation between the coronal upflows and spectroscopic signatures in TR and chromospheric lines observed with IRIS. The C II 1335.71 Å line is marginally blue-shifted in the upflows compared to in the AR core, Si IV 1393.75 Å is less red-shifted, and Mg II k2 shows a positive asymmetry, which may be interpreted as signatures of upflows.

By examining the evolution of underlying photospheric magnetic field, Su et al. (2012) identified clear signatures of flux cancellation around one footpoint of an AR loop. Fast jet-like upflows were found to initiate from the footpoint, and they are accompanied by transient brightenings in EUV images. However, no evident signature was found in images of the low chromosphere. They suggested that these upflows result from magnetic reconnection at the height of the upper chromosphere. Liu and Su (2014) found similar results, and they proposed that the intermittent upflows are produced by reconnection between small-scale emerging bipoles and pre-existing open-field structures at AR boundaries.

Recent observations by the *Parker Solar Probe* (PSP: Fox et al., 2016) have revealed quasi-periodic Type-III radio bursts that are well correlated with coronal intensity variations at the footpoints of AR loops, suggesting electron acceleration during impulsive reconnection process around the loop footpoints (Cattell et al., 2020). It is unclear whether these radio bursts are signatures of the reconnection processes that generate the AR upflows, but Harra et al. (2021) have found that a radio noise storm during PSP Encounter 2 (between 31 March and 4 April 2019) likely originates in the expansion of the upflow region at the boundary of the only AR on the visible disk during that period.

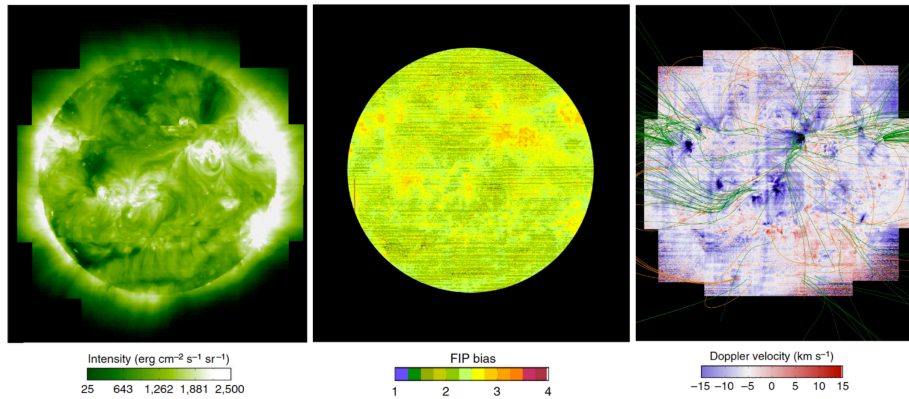


**Figure 13.** Source regions of the slow solar wind (Brooks, Ugarte-Urra, and Warren, 2015). From left to right: full-Sun images of the Fe XIII 202.04 Å line intensity, Si/S FIP bias and Fe XIII 202.04 Å Doppler shift. Some open (green) and closed (orange) field lines are overlaid on the Dopplergram.

### 3.4. Connection to the Solar Wind

The upflows are generally found at the edges of ARs, where EUV spectral lines formed at typical coronal temperatures often show reduced emission. The electron density and temperature there are both lower than those in the cores of ARs (Doschek et al., 2008). Interestingly, coronal holes also show reduced coronal emission, lower electron density, and lower temperature compared to neighboring quiet-Sun regions. These similarities between AR edges and coronal holes suggest that AR boundaries might also be source regions of the solar wind. Indeed, Kojima et al. (1999) found that low-speed solar-wind streams appear to be associated with regions of large magnetic-flux expansion in the vicinity of ARs. This association was confirmed by Ko et al. (2006), who compared the coronal electron temperature and abundances in the vicinity of an AR with in-situ measurements of the slow solar wind.

Magnetic-field extrapolations have been performed to understand the magnetic-field structures associated with the persistent upflows. Although a few investigations showed that a portion of the upflows may be guided by large-scale magnetic loops and eventually flow downward to the other footpoints of the loops (e.g. Boutry et al., 2012), most studies clearly demonstrated a close association of at least some of these upflows with open-field lines originating from AR boundaries (e.g. Marsch, Wiegelmann, and Xia, 2004; Sakao et al., 2007; Harra et al., 2008; Marsch et al., 2008; Baker et al., 2009). van Driel-Gesztelyi et al. (2012) performed both local magnetic-field extrapolations for individual ARs and global potential-field source-surface modeling. They found that a part of the AR upflows are confined in closed-field structures, and that the other part of the upflows are associated with field lines extending to the source surface from a coronal null point. This association strongly suggests that these AR upflows likely flow outward into interplanetary space and become part of the slow solar wind. However, Culhane et al. (2014) found that their studied

AR was completely covered by the closed field lines below the source surface, while the in-situ measurements, combined with the back-mapping technique, strongly suggest the origin of a slow-wind stream from the vicinity of this AR. To solve this apparent inconsistency, Mandrini et al. (2014) proposed a two-step reconnection process. After the first reconnection between the expanding AR loops and neighboring large-scale loops, new large-scale loops connecting the AR upflow and a distant location are formed. These loops then reconnect with open-field lines from a coronal hole around a coronal null point, releasing plasma of the AR upflow into interplanetary space. Harra et al. (2017) have also shown that the upflowing plasma could be released through interchange reconnection if the upflow-hosting ARs are close to an open-field region.

Chemical composition could be used to establish a link between some structures in the interplanetary solar wind and their source regions in the solar corona (e.g. Feldman and Widing, 2003; Song and Yao, 2020). Chemical elements with a first ionization potential (FIP) below and above  $\approx 10$  eV are often called low-FIP and high-FIP elements, respectively. It is well-known that the relative abundance of a low-FIP element to a high-FIP element is generally enhanced in the slow solar wind relative to its photospheric value by a factor of three to four. This factor is called the FIP bias. Spectroscopic observations at EUV wavelengths can be used to measure the FIP bias in the solar corona. Based on *Hinode*/EIS observations, Brooks and Warren (2011) found that the ratio of low-FIP Si and high-FIP S is enhanced by a factor of three to four at the locations of AR upflows. A similar ratio was found in the in-situ measurements of solar wind a few days later, providing evidence for a connection between the observed solar-wind stream and the AR upflows. In a following study, Brooks, Ugarte-Urra, and Warren (2015) applied a similar technique to the EIS data obtained through a full-Sun mosaic observation campaign and obtained a full-Sun composition (FIP bias) map. After comparing this composition map with the simultaneously obtained full-Sun Dopplergram and the global magnetic-field topology, they identified multiple locations of AR upflows as source regions of the slow solar wind (Figure 13).

Using the technique of double-Gaussian fit, Brooks and Warren (2012) decomposed the two components of the coronal line profiles observed at the boundaries of an AR. They found that the FIP bias for the high-speed upflow component is also in the range of three to five, suggesting that the high-speed component may also contribute to the slow solar wind. The complexity of the outflow components contributing to the solar wind was also highlighted by Brooks et al. (2020), who used *Hi-C* (Rachmeler et al., 2019) high spatial resolution images at  $172 \text{ \AA}$  to try to isolate the upflows cleanly from the cooler fan loops. Their results suggest that the variability in solar-wind composition measurements might be explained by activity in the source region.

By applying the technique of Doppler dimming to the spectra obtained with SOHO/UVCS in the height range of 1.5 to 2.3 solar radii from the solar center, Zangrilli and Poletto (2012) and Zangrilli and Poletto (2016) identified coronal outflows at the edges of ARs, and they found an increase of the outflow speed from  $\approx 50 \text{ km s}^{-1}$  at 1.5 solar radii to  $\approx 150 \text{ km s}^{-1}$  at 2.5 solar radii. Since the speeds at 1.5 solar radii are generally smaller than those of the secondary components in EIS observations, it is possible that the fast upflows corresponding

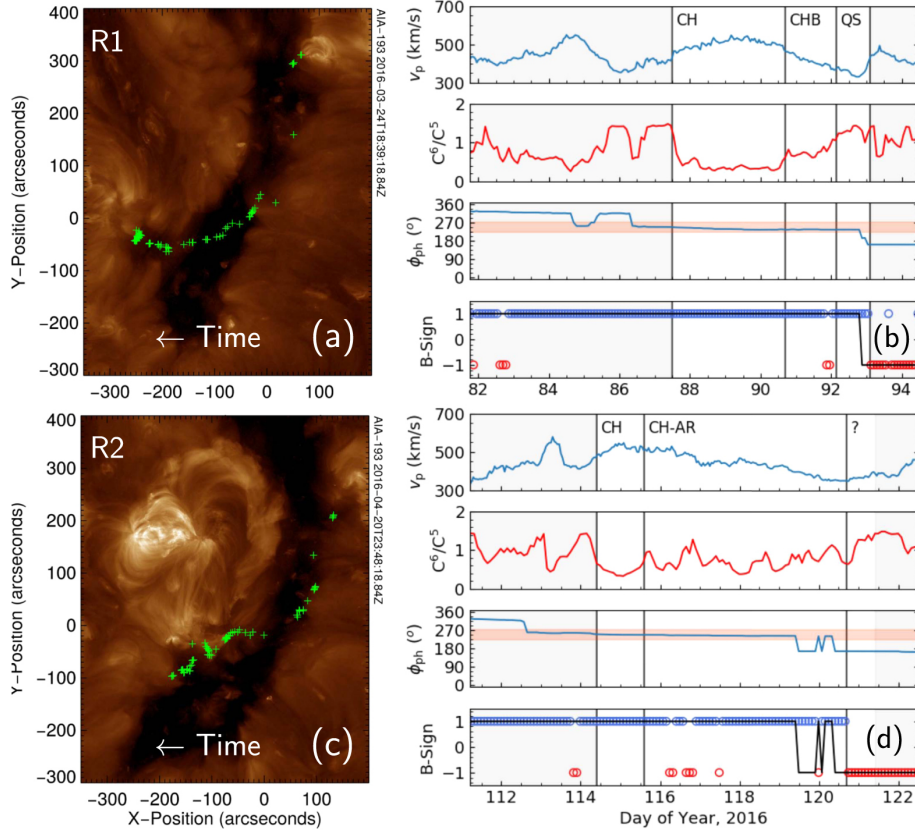


**Figure 14.** Left: AIA 193 Å images taken during two solar rotations (Macneil et al., 2019). The solar wind source points are overlotted on the images. Right: time series of several solar-wind parameters, with associated source regions labeled and separated by vertical lines. In panels b or d the first two rows correspond to the solar-wind velocity and  $C^{6+}/C^{5+}$ , respectively. The third row shows the sourcepoint longitude for each mapped data point. The orange bar indicates longitudes corresponding to the vicinity of the CH. The fourth row shows the magnetic-field polarity of the radial component of the interplanetary magnetic field (circles) and the corresponding PFSS magnetic-field polarity for each mapped data point (black line). Reproduced by permission of the AAS.

to the secondary components mostly supply mass to the corona and do not directly escape to the interplanetary space. Instead, the primary components in EIS observations, with a blue shift of about  $10 \text{ km s}^{-1}$  (e.g. Tian et al., 2011b), may be the major source of the outflows detected by UVCS. It is also possible that what UVCS measured is an average speed, meaning that the weak and transient high-speed upflows may have been smeared out over the course of temporal or spatial sampling.

Longer-term measurements are also helpful for understanding the linkage between the upflows and the solar wind. By comparing the synoptic photospheric magnetograms and the time sequences of solar-wind parameters, He et al. (2010) concluded that the upflowing plasma at an AR boundary may evolve into an intermediate-speed solar-wind stream observed near the Earth.



This solar-wind stream has a speed of about  $400 \text{ km s}^{-1}$ , and an intermediate temperature and density if comparing to the typical fast and slow solar wind. In another study by Janardhan, Tripathi, and Mason (2008), the authors managed to establish a link between an extremely slow ( $\leq 300 \text{ km s}^{-1}$ ) solar-wind stream measured in interplanetary space and an evolving low-emission coronal region located near an AR. They claimed that interchange reconnection between the AR loops and surrounding open fields leads to a reduction in the area of the open-field region, which would result in a smaller solar-wind velocity. With the help of the potential-field source-surface (PFSS) model, Liewer, Neugebauer, and Zurbuchen (2004) ballistically mapped several solar-wind streams back to the source surface and then to the photosphere. They found that these solar-wind streams generally can be traced back to dark areas in EUV and soft X-ray images at the edges of ARs. Fazakerley, Harra, and van Driel-Gesztelyi (2016) tracked a Carrington rotation that had coronal holes and active regions. The solar wind was linked back to the features on the Sun, using ballistic back mapping and PFSS modelling. They found short periods of enhanced-velocity solar wind at the boundary of slow and fast wind streams, which are related to ARs that are located beside coronal holes. The neighbours of ARs are important in terms of how the solar wind is created. Figure 14 shows an example of connecting remote sensing data that are showing regions of upflows in a coronal hole and an AR, with the solar-wind measurements (Macneil et al., 2019). These authors examined two solar rotations, one with the quiet Sun and coronal hole only, and during the next rotation an AR has emerged, making it ideal to compare the two different situations. Their observations indicate that the features that emerge in the AR-associated wind are consistent with an increased occurrence of interchange reconnection during solar-wind production, compared with the initial quiet-Sun case. Back-mapping the solar wind to the source surface to trace solar wind source regions has also been trialed on *Hinode* and ACE observations as a science preparation for *Solar Orbiter* (Stansby et al., 2020), and the authors discussed some of the difficulties involved in interpreting the composition measurements. A direct link between solar-wind streams and their coronal source regions may also be achieved in a different way by using the Wang–Sheeley–Arge (WSA) model (Wang and Sheeley, 1990; Arge and Pizzo, 2000). Using the WSA model, Slemzin et al. (2013) have also identified locations of AR upflows as the source regions of slow solar-wind streams.

Tracing the solar wind back to the Sun from 1999 to 2008, Fu et al. (2015) classified the solar wind by its source-region types with the EUV images and photospheric magnetograms taken by SOHO. They found that about half of the solar-wind streams come from AR regions during the solar maximum. The charge states, FIP bias and helium abundance are significantly different for the solar wind coming from ARs, the quiet Sun, and coronal-hole regions (Fu et al., 2017, 2018). Their results further indicate that the reconnection between the open magnetic-field lines and closed loops may play a major role in the generation of the AR-associated wind.

#### 4. Upflows from CME-Induced Dimmings

When coronal mass ejections (CMEs) leave the Sun, often we see reduced emission of the corona, most noticeably at EUV and soft X-ray wavelengths (e.g. Hudson, Acton, and Freeland, 1996; Sterling and Hudson, 1997; Dissauer et al., 2018, 2019). This phenomenon is called coronal dimming, and a dimming region is sometimes called a transient coronal hole. Statistical studies show that more than half of the frontside CMEs are associated with dimmings (Reinard and Biesecker, 2008; Bewsher, Harrison, and Brown, 2008). There are at least two types of coronal dimmings: core (or twin) dimmings and secondary dimmings. Core dimmings usually refer to small regions of greatly reduced coronal emission near the eruption sites of CMEs. They are generally believed to mark the footpoints of ejected flux ropes, and they could last for more than ten hours (e.g. Hudson, Acton, and Freeland, 1996; Vanninathan et al., 2018; Chen et al., 2019a; Xing, Cheng, and Ding, 2020). Secondary dimmings, which may result from stretching of the magnetic-field lines or reconnection of the erupting magnetic field with the surrounding structures, often show a less prominent intensity decrease and a quicker recovery (e.g. Thompson et al., 2000; Mandrini et al., 2007; Zheng, Chen, and Wang, 2016; Vanninathan et al., 2018). Note that some dimmings are likely not associated with CMEs, e.g. long-duration remote dimmings associated with confined circular-ribbon flares (Zhang and Zheng, 2020) and dimmings at the peripheries of emerging flux regions (Zhang et al., 2012). Here we focus on CME-induced dimmings. Spectroscopic observations often reveal an obvious density decrease in these dimming regions (Harrison and Lyons, 2000; Harrison et al., 2003; Tian et al., 2012b). In addition, the peak temperature of the differential-emission-measure curve appears not to change when a dimming occurs (Tian et al., 2012a). These results demonstrate that coronal dimming is mainly due to mass loss rather than temperature change. Signatures of coronal dimming are also present in the Sun-as-a-star spectra taken by the *EUV Variability Experiment* (EVE: Woods et al., 2012) onboard SDO (Mason et al., 2014).

There are only a few spectroscopic investigations of coronal dimmings. Using CDS observations, Harra and Sterling (2001) reported an obvious blue shift in coronal and TR lines in coronal dimming regions. At least a few coronal dimming events have been caught by the EIS spectrograph. These observations often reveal a prominent blue shift of coronal emission lines in dimming regions, normally in the range of  $\approx 10\text{--}50\text{ km s}^{-1}$ , with an average of about  $20\text{ km s}^{-1}$  when a SGF is performed (Harra et al., 2007, 2011). These blue shifts appear to be very similar to those at AR boundaries, and they likely represent systematic plasma upflows along the field lines opened by CMEs. The strongest blue shifts are found at the footpoints of disrupted coronal loops (Harra et al., 2007; Attrill et al., 2010). The blue shift appears to be positively correlated with the depression of coronal emission and magnetic-field strength in the photosphere (Jin et al., 2009). In addition, the spectral-line profiles are found to be broadened compared to the line profiles in the pre-eruption phase and outside dimming regions. The large line width has been interpreted as a result of amplified Alfvén

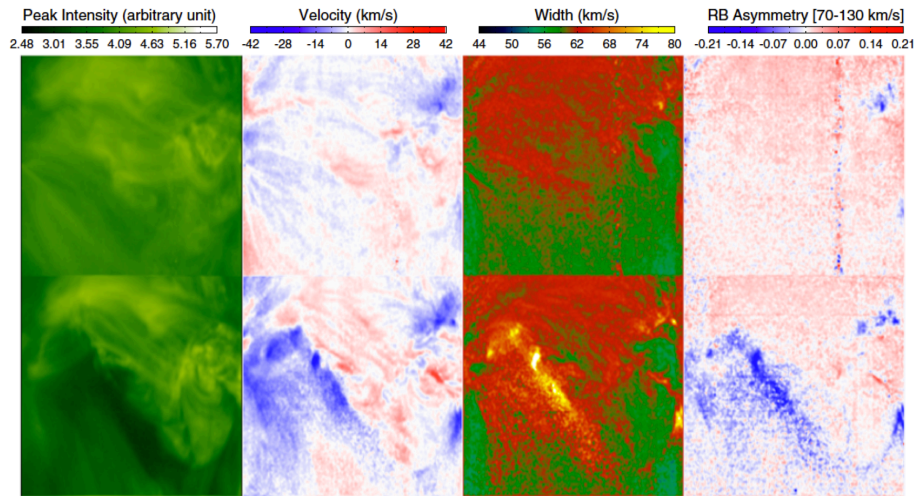


**Figure 15.** Maps of the peak intensity, Doppler shift, and line width derived from a SGF, and RB asymmetry in the velocity interval of  $70-130 \text{ km s}^{-1}$  for the Fe XIII 202.04 Å line (Tian et al., 2012b). The first and second rows show observational results before and after a CME eruption, respectively. The FOV of each image is about  $250'' \times 250''$ . The same dataset has also been analyzed by Harra et al. (2007) and Jin et al. (2009). Reproduced by permission of the AAS.

wave amplitude (McIntosh, 2009) or inhomogeneity of flow velocities along the LOS (Dolla and Zhukov, 2011).

Similarly, the coronal line profiles have been found to be asymmetric in dimming regions. Using the technique of RB-asymmetry analysis introduced by De Pontieu et al. (2009), McIntosh, De Pontieu, and Leamon (2010) found a couple of small patches in the dimming region behind an erupted halo CME where the Fe XIII 202.04 Å line profile is slightly enhanced at the blue wing. Note that they used the SGF to determine the line centroid when performing the RB-asymmetry analysis, which tends to underestimate the degree of the actual profile asymmetry (Tian et al., 2011b). As demonstrated by Tian et al. (2011b), the secondary component can be more accurately resolved if the wavelength position of the peak spectral intensity is used to determine the line centroid. Tian et al. (2012b) applied this improved RB-asymmetry technique to the same dataset, and found much more prominent and pervasive blueward asymmetries in dimming regions. As shown in Figure 15, when a dimming occurs, we see not only the intensity depression, obvious blue shift, and enhanced line width derived from a SGF, but also clear blueward asymmetry. The strongest blueward asymmetries appear in areas of strongest intensity reduction. Detailed analyses of the line profiles suggest that a single Gaussian function normally cannot fit the observed line profiles in dimming regions well. Instead, a double-Gaussian fit appears to approximate the observed line profiles very well. So, similar to AR boundaries, the coronal emission in dimming regions also consists of at least two emission components: a nearly stationary background component and a weak high-speed upflow component. The secondary component has an upward speed of about  $100 \text{ km s}^{-1}$ . The intensity ratio of the two components is often about

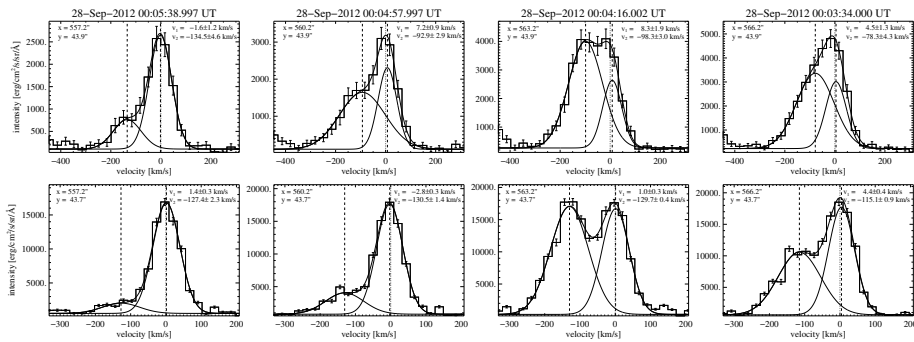


**Figure 16.** Line profiles of Fe XIII 202.04 Å (upper panels) and Fe XV 284.16 Å (lower panels) at four pixels within a dimming region (Veronig et al., 2019). The three smooth curves in each panel represent the two Gaussian components and their sum. Reproduced by permission of the AAS.

5–15%, but at some pixels it could be as high as 40%. Tian et al. (2012b) also found that the SGF blue shift, line width, and blueward asymmetry are all strongly correlated, indicating that the  $\approx 20 \text{ km s}^{-1}$  blue shift and enhanced line width derived from a SGF are caused at least partly by the superposition of the two components. So it appears clear that a fraction of the coronal plasma in dimming regions flows upward at a speed of the order of  $\approx 100 \text{ km s}^{-1}$ . Recent EUV-imaging observations with AIA have clearly revealed upflows with speeds of  $\approx 70\text{--}140 \text{ km s}^{-1}$  from a CME footpoint in a dimming region (Lörinčák et al., 2021), confirming the finding of Tian et al. (2012b).

Similar blueward asymmetry and a high-speed upflow component have been commonly observed in other dimming events. Chen, Ding, and Chen (2010) reported an expanding dimming event with a leading edge/ridge of enhanced line width. Tian et al. (2012b) examined the asymmetry of the coronal spectra and found clear blueward asymmetries along the whole ridge and in the obvious dimming regions behind it. In a recent study, Veronig et al. (2019) found that at the growing dimming border the upflow component is so strong that the spectra even show distinct double components (Figure 16). At some pixels the upflow component even dominates over the nearly stationary component. Such line profiles can be decomposed with a high degree of accuracy through a double-Gaussian fit.

What is the significance of these upflows? Dimming regions are often called transient coronal holes, as the coronal magnetic-field lines are transiently opened by the CME ejecta. So a large fraction of these upflows likely flow outward along the opened field lines and eventually become solar-wind streams following the CME ejecta. In this sense, a dimming region should be regarded as a source region of the solar wind, similar to AR boundaries and coronal holes (McIntosh, 2009; Tian et al., 2012b). The enhanced nonthermal broadening may be contributed by both the superposition of different emission components and the growing Alfvén wave amplitude in the open-field and low-density coronal environment. The momentum flux resulting from the high-speed upflows may act as a secondary momentum source, and thus it may impact the kinematics of the associated CMEs (McIntosh, De Pontieu, and Leamon, 2010). It is also

possible that these upflows continuously feed the associated CMEs (Harra et al., 2007). Using the density sensitive line pair Fe XIII 196.55 Å/202.04 Å, Veronig et al. (2019) derived an electron density of  $2.25 \times 10^9 \text{ cm}^{-3}$  for the upflow component. They then estimated a mass-loss rate due to the upflows, which is about  $8 \times 10^{11} \text{ g s}^{-1}$  and comparable to the mass-increase rate of the associated CME inferred from coronagraph observations. Thus, the upflows may become part of the CME. In addition, since a dimming region will eventually recover to the pre-eruption state, part of these upflows might provide mass to refill the corona after the eruption of CMEs (Tian et al., 2012b).

Besides these prevalent high-speed upflows that appear to show no obvious temperature dependence, clear temperature-dependent upflows associated with dimmings have also been identified. For instance, Imada et al. (2007) identified an upflow with a speed increasing from  $\approx 15 \text{ km s}^{-1}$  at  $10^{4.9} \text{ K}$  to  $\approx 160 \text{ km s}^{-1}$  at  $10^{6.3} \text{ K}$  at the edge of a dimming region. With the RB-asymmetry technique, Tian et al. (2012b) detected several more temperature-dependent upflows, but all in very small areas immediately outside the (deepest) dimming regions. These temperature-dependent upflows are likely evaporation flows induced by interaction between the stretching field lines in dimming regions and adjacent magnetic-field structures.

Dimmings have been linked to magnetic-cloud materials. Harra et al. (2011) used upflow measurements to determine accurately where the dimming occurred through a velocity-difference method. They used this to determine the maximum amount of magnetic field that could end up in a magnetic cloud. The magnetic-cloud measurements and modelling determined that the magnetic flux in the dimming region is consistent with the magnetic-cloud data.

## 5. Summary and Future Perspectives

In the past two to three decades, EUV/FUV spectroscopic observations have largely changed our view of the upper solar atmosphere. With these dedicated observations, highly structured upflows and downflows with varying magnitudes at different temperatures have been identified in various regions on the Sun. On large scales these flows appear to be quasi-steady and long-lasting, possibly indicating a continuous global plasma circulation (Marsch et al., 2008). Systematic upflows in the upper TR and corona have been commonly believed to be signatures of the nascent solar wind. High-cadence observations and detailed analyses of the spectral-line profiles suggest that there are intermittent high-speed upflow components with a wide range of temperatures and a relatively slow cooling downflow component mostly at TR temperatures. These observations indicate that the upper atmosphere is not a static and magnetically stratified layer, but rather a dynamic interface revealing a continuous mass cycling between the chromosphere and corona/solar wind.

We have presented an extended overview of plasma flows observed by the EUV/FUV spectrographs of *Hinode*/EIS, IRIS, SOHO/SUMER, and SOHO/CDS, with an emphasis on the upflows seen in the network structures of the quiet Sun

and coronal holes, boundaries of ARs, and CME-induced dimming regions. Despite significant advances in the research of these plasma flows, several important unresolved issues remain and require further investigations.

For the quiet Sun and coronal holes, there is still no consensus on the physical mechanisms behind the observed temperature dependence of the Doppler shift. It is commonly believed that this temperature dependency is a consequence of coronal heating (Peter, Gudiksen, and Nordlund, 2006; Hansteen et al., 2010). So more realistic numerical simulations of coronal heating should be performed to better understand this temperature dependency. In addition, the exact temperature at which the net Doppler shift changes sign is still unclear, mainly because there are no strong emission lines formed between the redshift-dominated temperatures of  $\log T \leq 5.4$  and the blueshift-dominated temperatures of  $\log T \geq 5.8$  in the SUMER spectral range. Considering this, the strong Ne VII 465 Å line formed around  $\log T = 5.7$  is highly recommended for future EUV instruments aiming at high-resolution observations of the quiet Sun and coronal holes (Tian, 2017).

For the upflows at AR boundaries, at least three important questions or issues need to be addressed in the future. First, it is clear now that both flows and waves are present at AR boundaries. However, we still do not know how exactly the upflows and waves are generated and related. So far only a few numerical models exist and they are not fully compatible with observational characteristics. Although a few case studies have shown local heating and injection of individual fast upflows at loop footpoints (e.g. Li and Peter, 2019), detailed observations of the generation, propagation, and heating of individual upflow events are generally missing. Second, the contribution of the fast upflows to coronal heating is still highly debated. Contradictory conclusions have been reached based on different approaches. Third, although a few studies have managed to trace several slow solar-wind streams back to the coronal sources, a one-to-one connection between coronal upflows and interplanetary solar-wind streams still cannot be established routinely. In the future, more advanced MHD simulations should be performed to understand the generation, propagation, and energization of the upflows and waves. In addition, the *Spectral Imaging of the Coronal Environment* (SPICE: SPICE Consortium et al., 2020) instrument onboard the newly launched *Solar Orbiter* mission (Müller et al., 2020) has the capability of sampling several strong emission lines formed at both TR and coronal temperatures at a high spatial and temporal resolution. Combined observations between SPICE and the 4-m *Daniel K. Inouye Solar Telescope* (DKIST) will likely reveal new insights into the generation and propagation of the upflows/waves as well as their role in the energization of the coronal plasma. Having a mission such as *Solar Orbiter* in an orbit away from the Earth's orbit will also allow 3D spectroscopy by combining *Solar Orbiter*/SPICE with the Earth-orbiting *Hinode*/EIS and IRIS missions. A main goal of the *Solar Orbiter* mission is to trace the interplanetary solar-wind streams back to their sources in the corona more accurately and routinely by combining imaging and spectroscopic observations with in-situ measurements. FIP bias measurements both spectroscopically and in situ will form a significant part of this work. New insight could also be obtained through observations with a future spectrometer, the *Solar-C EUV High-Throughput Spectroscopic Telescope*

(EUVST, Shimizu et al., 2019), which has been approved by JAXA. *Solar-C/EUVST* will provide near continuous spectral measurements throughout the solar atmosphere at similar spatial resolutions. The spatial resolution will be around seven times better than that of *Hinode/EIS*, and the temperature coverage allows us to observe seamlessly from the chromosphere ( $\approx 10,000$  Kelvin), to the corona ( $\approx 1$  million Kelvin), and flare plasmas ( $\approx 10$  million kelvin). Normally magnetic-field extrapolations are required to guide our understanding of the corona–solar-wind connection. With recently developed promising techniques of coronal magnetic-field measurements (Yang et al., 2020a,b; Li et al., 2015, 2016; Si et al., 2020; Landi et al., 2020), magnetic-field extrapolations will likely improve and thus help establish a more accurate connection between the coronal upflows and interplanetary solar-wind streams. In addition, the coronal magnetic field measurements from DKIST will allow us to fully understand the coronal magnetic field rather than rely completely on models. These new facilities will revolutionize our understanding of the energy transport in the solar atmosphere (Velli et al., 2020).

Formation mechanisms of the upflows in CME-induced dimming regions, and their potential role in solar-wind formation and impact on CME evolution, are still poorly understood. This is mainly due to the infrequent spectroscopic observations of dimmings because of the small fields of view and lower cadence of the slit scans. Possibly, future instrumentation should aim at full-disk spectroscopic imaging with a wide temperature coverage to catch a large number of dimming events. In the *Solar Orbiter* era, we also expect that the linkage between dimming regions and solar-wind streams will be made more easily than before.

**Acknowledgments** H. Tian is supported by NSFC grants 11825301 and 11790304. The work of D. H. Brooks was performed under contract to the Naval Research Laboratory and was funded by the NASA *Hinode* program. D. Baker is funded under STFC consolidated grant number ST/S000240/1. L. Xia is supported by NSFC grants 41974201 and 41627806. H. Tian acknowledges support from the UCL-PKU strategic partner funds during his visit to MSSL. This article is based upon the AAS/SPD Karen Harvey Prize Lecture of 2020, the presentation file of which is available at <http://spd.aas.org/prizes/harvey/previous>.

**Disclosure of Potential Conflicts of Interest** The authors declare that they have no conflicts of interest.

## References

- Aiouaz, T.: 2008, Evidence of Relentless Reconnections at Boundaries of Supergranular Network Lanes in Quiet Sun and Coronal Hole. *Astrophys. J.* **674**, 1144. DOI. ADS.
- Aiouaz, T., Peter, H., Lemaire, P.: 2005, The correlation between coronal Doppler shifts and the supergranular network. *Astron. Astrophys.* **435**, 713. DOI. ADS.
- Arge, C.N., Pizzo, V.J.: 2000, Improvement in the prediction of solar wind conditions using near-real time solar magnetic field updates. *J. Geophys. Res.* **105**, 10465. DOI. ADS.
- Attrill, G.D.R., Harra, L.K., van Driel-Gesztelyi, L., Wills-Davey, M.J.: 2010, Revealing the Fine Structure of Coronal Dimmings and Associated Flows with *Hinode/EIS*. Implications for Understanding the Source Regions of Sustained Outflow Following CMEs. *Solar Phys.* **264**, 119. DOI. ADS.
- Baker, D., van Driel-Gesztelyi, L., Green, L.M.: 2012, Forecasting a CME by Spectroscopic Precursor? *Solar Phys.* **276**, 219. DOI. ADS.

- Baker, D., van Driel-Gesztelyi, L., Mandrini, C.H., Démoulin, P., Murray, M.J.: 2009, Magnetic Reconnection along Quasi-separatrix Layers as a Driver of Ubiquitous Active Region Outflows. *Astrophys. J.* **705**, 926. DOI ADS.
- Baker, D., Janvier, M., Démoulin, P., Mandrini, C.H.: 2017, Apparent and Intrinsic Evolution of Active Region Upflows. *Solar Phys.* **292**, 46. DOI ADS.
- Bewsher, D., Harrison, R.A., Brown, D.S.: 2008, The relationship between EUV dimming and coronal mass ejections. I. Statistical study and probability model. *Astron. Astrophys.* **478**, 897. DOI ADS.
- Boutry, C., Buchlin, E., Vial, J.-C., Régnier, S.: 2012, Flows at the Edge of an Active Region: Observation and Interpretation. *Astrophys. J.* **752**, 13. DOI ADS.
- Bradshaw, S.J., Klimchuk, J.A.: 2015, Chromospheric Nanoflares as a Source of Coronal Plasma. II. Repeating Nanoflares. *Astrophys. J.* **811**, 129. DOI ADS.
- Bradshaw, S.J., Aulanier, G., Del Zanna, G.: 2011, A Reconnection-driven Rarefaction Wave Model for Coronal Outflows. *Astrophys. J.* **743**, 66. DOI ADS.
- Brooks, D.H., Warren, H.P.: 2011, Establishing a Connection Between Active Region Outflows and the Solar Wind: Abundance Measurements with EIS/Hinode. *Astrophys. J. Lett.* **727**, L13. DOI ADS.
- Brooks, D.H., Warren, H.P.: 2012, The Coronal Source of Extreme-ultraviolet Line Profile Asymmetries in Solar Active Region Outflows. *Astrophys. J. Lett.* **760**, L5. DOI ADS.
- Brooks, D.H., Ugarte-Urra, I., Warren, H.P.: 2015, Full-Sun observations for identifying the source of the slow solar wind. *Nature Comm.* **6**, 5947. DOI ADS.
- Brooks, D.H., Winebarger, A.R., Savage, S., Warren, H.P., De Pontieu, B., Peter, H., Cirtain, J.W., Golub, L., Kobayashi, K., McIntosh, S.W., McKenzie, D., Morton, R., Rachmeler, L., Testa, P., Tiwari, S., Walsh, R.: 2020, The Drivers of Active Region Outflows into the Slow Solar Wind. *Astrophys. J.* **894**, 144. DOI ADS.
- Bryans, P., Young, P.R., Doschek, G.A.: 2010, Multiple Component Outflows in an Active Region Observed with the EUV Imaging Spectrometer on Hinode. *Astrophys. J.* **715**, 1012. DOI ADS.
- Bryans, P., McIntosh, S.W., De Moortel, I., De Pontieu, B.: 2016, On the Connection between Propagating Solar Coronal Disturbances and Chromospheric Footpoints. *Astrophys. J. Lett.* **829**, L18. DOI ADS.
- Cattell, C., Glesener, L., Leiran, B., Goetz, K., Martínez Oliveros, J.C., Badman, S.T., Pulupa, M., Bale, S.D.: 2020, Periodicities in an active region correlated with Type III radio bursts observed by Parker Solar Probe, arXiv:2009.10899. ADS.
- Chen, F., Ding, M.D., Chen, P.F.: 2010, Spectroscopic Analysis of an EIT Wave/dimming Observed by Hinode/EIS. *Astrophys. J.* **720**, 1254. DOI ADS.
- Chen, H., Yang, J., Ji, K., Duan, Y.: 2019a, Observational Analysis on the Early Evolution of a CME Flux Rope: Preflare Reconnection and Flux Rope's Footpoint Drift. *Astrophys. J.* **887**, 118. DOI ADS.
- Chen, Y., Tian, H., Huang, Z., Peter, H., Samanta, T.: 2019b, Investigating the Transition Region Explosive Events and Their Relationship to Network Jets. *Astrophys. J.* **873**, 79. DOI ADS.
- Cirtain, J.W., Golub, L., Lundquist, L., van Ballegooyen, A., Savcheva, A., Shimojo, M., DeLuca, E., Tsuneta, S., Sakao, T., Reeves, K., Weber, M., Kano, R., Narukage, N., Shibasaki, K.: 2007, Evidence for Alfvén Waves in Solar X-ray Jets. *Science* **318**, 1580. DOI ADS.
- Culhane, J.L., Harra, L.K., James, A.M., Al-Janabi, K., Bradley, L.J., Chaudry, R.A., Rees, K., Tandy, J.A., Thomas, P., Whillock, M.C.R., Winter, B., Doschek, G.A., Korendyke, C.M., Brown, C.M., Myers, S., Mariska, J., Seely, J., Lang, J., Kent, B.J., Shaughnessy, B.M., Young, P.R., Simnett, G.M., Castelli, C.M., Mahmoud, S., Mapson-Menard, H., Probyn, B.J., Thomas, R.J., Davila, J., Dere, K., Windt, D., Shea, J., Hagood, R., Moye, R., Hara, H., Watanabe, T., Matsuzaki, K., Kosugi, T., Hansteen, V., Wikstol, Ø.: 2007, The EUV Imaging Spectrometer for Hinode. *Solar Phys.* **243**, 19. DOI ADS.
- Culhane, J.L., Brooks, D.H., van Driel-Gesztelyi, L., Démoulin, P., Baker, D., DeRosa, M.L., Mandrini, C.H., Zhao, L., Zurbuchen, T.H.: 2014, Tracking Solar Active Region Outflow Plasma from Its Source to the Near-Earth Environment. *Solar Phys.* **289**, 3799. DOI ADS.
- Dadashi, N., Teriaca, L., Solanki, S.K.: 2011, The quiet Sun average Doppler shift of coronal lines up to 2 MK. *Astron. Astrophys.* **534**, A90. DOI ADS.
- Dammasch, I.E., Wilhelm, K., Curdt, W., Hassler, D.M.: 1999, The NE BT VIII ( $\lambda$  770) resonance line: solar wavelengths determined by SUMER on SOHO. *Astron. Astrophys.* **346**, 285. ADS.



- Dammasch, I.E., Curdt, W., Dwivedi, B.N., Parenti, S.: 2008, The redshifted footpoints of coronal loops. *Ann. Geophys.* **26**, 2955. DOI. ADS.
- de Moortel, I.: 2009, Longitudinal Waves in Coronal Loops. *Space Sci. Rev.* **149**, 65. DOI. ADS.
- De Moortel, I., Ireland, J., Walsh, R.W.: 2000, Observation of oscillations in coronal loops. *Astron. Astrophys.* **355**, L23. ADS.
- De Pontieu, B., McIntosh, S.W.: 2010, Quasi-periodic Propagating Signals in the Solar Corona: The Signature of Magnetoacoustic Waves or High-velocity Upflows? *Astrophys. J.* **722**, 1013. DOI. ADS.
- De Pontieu, B., McIntosh, S., Hansteen, V.H., Carlsson, M., Schrijver, C.J., Tarbell, T.D., Title, A.M., Shine, R.A., Suematsu, Y., Tsuneta, S., Katsukawa, Y., Ichimoto, K., Shimizu, T., Nagata, S.: 2007, A Tale of Two Spicules: The Impact of Spicules on the Magnetic Chromosphere. *Pub. Astron. Soc. Japan* **59**, S655. DOI. ADS.
- De Pontieu, B., McIntosh, S.W., Hansteen, V.H., Schrijver, C.J.: 2009, Observing the Roots of Solar Coronal Heating—in the Chromosphere. *Astrophys. J. Lett.* **701**, L1. DOI. ADS.
- De Pontieu, B., McIntosh, S.W., Carlsson, M., Hansteen, V.H., Tarbell, T.D., Boerner, P., Martinez-Sykora, J., Schrijver, C.J., Title, A.M.: 2011, The Origins of Hot Plasma in the Solar Corona. *Science* **331**, 55. DOI. ADS.
- De Pontieu, B., Title, A.M., Lemen, J.R., Kushner, G.D., Akin, D.J., Allard, B., Berger, T., Boerner, P., Cheung, M., Chou, C., Drake, J.F., Duncan, D.W., Freeland, S., Heyman, G.F., Hoffman, C., Hurlburt, N.E., Lindgren, R.W., Mathur, D., Rehse, R., Sabolish, D., Seguin, R., Schrijver, C.J., Tarbell, T.D., Wülser, J.-P., Wolfson, C.J., Yanari, C., Mudge, J., Nguyen-Phuc, N., Timmons, R., van Bezooijen, R., Weingrod, I., Brookner, R., Butcher, G., Dougherty, B., Eder, J., Knagenhjelm, V., Larsen, S., Mansir, D., Phan, L., Boyle, P., Cheimets, P.N., DeLuca, E.E., Golub, L., Gates, R., Hertz, E., McKillop, S., Park, S., Perry, T., Podgorski, W.A., Reeves, K., Saar, S., Testa, P., Tian, H., Weber, M., Dunn, C., Eccles, S., Jaeggli, S.A., Kankelborg, C.C., Mashburn, K., Pust, N., Springer, L., Carvalho, R., Kleint, L., Marmie, J., Mazmanian, E., Pereira, T.M.D., Sawyer, S., Strong, J., Worden, S.P., Carlsson, M., Hansteen, V.H., Leenaarts, J., Wiesmann, M., Aloise, J., Chu, K.-C., Bush, R.I., Scherrer, P.H., Brekke, P., Martinez-Sykora, J., Lites, B.W., McIntosh, S.W., Uitenbroek, H., Okamoto, T.J., Gummin, M.A., Auker, G., Jerram, P., Pool, P., Waltham, N.: 2014, The Interface Region Imaging Spectrograph (IRIS). *Solar Phys.* **289**, 2733. DOI. ADS.
- Del Zanna, G.: 2008, Flows in active region loops observed by Hinode EIS. *Astron. Astrophys.* **481**, L49. DOI. ADS.
- Del Zanna, G., Aulanier, G., Klein, K.-L., Török, T.: 2011, A single picture for solar coronal outflows and radio noise storms. *Astron. Astrophys.* **526**, A137. DOI. ADS.
- Démoulin, P., Baker, D., Mandrini, C.H., van Driel-Gesztelyi, L.: 2013, The 3D Geometry of Active Region Upflows Deduced from Their Limb-to-Limb Evolution. *Solar Phys.* **283**, 341. DOI. ADS.
- Dissauer, K., Veronig, A.M., Temmer, M., Podladchikova, T., Vanninathan, K.: 2018, On the Detection of Coronal Dimmings and the Extraction of Their Characteristic Properties. *Astrophys. J.* **855**, 137. DOI. ADS.
- Dissauer, K., Veronig, A.M., Temmer, M., Podladchikova, T.: 2019, Statistics of Coronal Dimmings Associated with Coronal Mass Ejections. II. Relationship between Coronal Dimmings and Their Associated CMEs. *Astrophys. J.* **874**, 123. DOI. ADS.
- Dolla, L.R., Zhukov, A.N.: 2011, On the Nature of the Spectral Line Broadening in Solar Coronal Dimmings. *Astrophys. J.* **730**, 113. DOI. ADS.
- Domingo, V., Fleck, B., Poland, A.I.: 1995, The SOHO Mission: an Overview. *Solar Phys.* **162**, 1. DOI. ADS.
- Doschek, G.A.: 2012, The Dynamics and Heating of Active Region Loops. *Astrophys. J.* **754**, 153. DOI. ADS.
- Doschek, G.A., Feldman, U., Bohlin, J.D.: 1976, Doppler wavelength shifts of transition zone lines measured in Skylab solar spectra. *Astrophys. J. Lett.* **205**, L177. DOI. ADS.
- Doschek, G.A., Warren, H.P., Mariska, J.T., Muglach, K., Culhane, J.L., Hara, H., Watanabe, T.: 2008, Flows and Nonthermal Velocities in Solar Active Regions Observed with the EUV Imaging Spectrometer on Hinode: A Tracer of Active Region Sources of Heliospheric Magnetic Fields? *Astrophys. J.* **686**, 1362. DOI. ADS.
- Edwards, S.J., Parnell, C.E., Harra, L.K., Culhane, J.L., Brooks, D.H.: 2016, A Comparison of Global Magnetic Field Skeletons and Active-Region Upflows. *Solar Phys.* **291**, 117. DOI. ADS.

- Fazakerley, A.N., Harra, L.K., van Driel-Gesztelyi, L.: 2016, An Investigation of the Sources of Earth-directed Solar Wind during Carrington Rotation 2053. *Astrophys. J.* **823**, 145. DOI ADS.
- Feldman, U., Widing, K.G.: 2003, Elemental Abundances in the Solar Upper Atmosphere Derived by Spectroscopic Means. *Space Sci. Rev.* **107**, 665. DOI ADS.
- Fox, N.J., Velli, M.C., Bale, S.D., Decker, R., Driesman, A., Howard, R.A., Kasper, J.C., Kinnison, J., Kusterer, M., Lario, D., Lockwood, M.K., McComas, D.J., Raouafi, N.E., Szabo, A.: 2016, The Solar Probe Plus Mission: Humanity’s First Visit to Our Star. *Space Sci. Rev.* **204**, 7. DOI ADS.
- Fu, H., Xia, L., Li, B., Huang, Z., Jiao, F., Mou, C.: 2014, Measurements of Outflow Velocities in on-disk Plumes from EIS/Hinode Observations. *Astrophys. J.* **794**, 109. DOI ADS.
- Fu, H., Li, B., Li, X., Huang, Z., Mou, C., Jiao, F., Xia, L.: 2015, Coronal Sources and In Situ Properties of the Solar Winds Sampled by ACE During 1999 - 2008. *Solar Phys.* **290**, 1399. DOI ADS.
- Fu, H., Madjarska, M.S., Xia, L., Li, B., Huang, Z., Wangguan, Z.: 2017, Charge States and FIP Bias of the Solar Wind from Coronal Holes, Active Regions, and Quiet Sun. *Astrophys. J.* **836**, 169. DOI ADS.
- Fu, H., Madjarska, M.S., Li, B., Xia, L., Huang, Z.: 2018, Helium abundance and speed difference between helium ions and protons in the solar wind from coronal holes, active regions, and quiet Sun. *Mon. Not. Roy. Astron. Soc.* **478**, 1884. DOI ADS.
- Galsgaard, K., Madjarska, M.S., Vanninathan, K., Huang, Z., Presmann, M.: 2015, Active region upflows. II. Data driven magnetohydrodynamic modelling. *Astron. Astrophys.* **584**, A39. DOI ADS.
- Gudiksen, B.V., Nordlund, Å.: 2005, An Ab Initio Approach to the Solar Coronal Heating Problem. *Astrophys. J.* **618**, 1020. DOI ADS.
- Hansteen, V.H., Hara, H., De Pontieu, B., Carlsson, M.: 2010, On Redshifts and Blueshifts in the Transition Region and Corona. *Astrophys. J.* **718**, 1070. DOI ADS.
- Hara, H., Watanabe, T., Harra, L.K., Culhane, J.L., Young, P.R., Mariska, J.T., Doschek, G.A.: 2008, Coronal Plasma Motions near Footpoints of Active Region Loops Revealed from Spectroscopic Observations with Hinode EIS. *Astrophys. J. Lett.* **678**, L67. DOI ADS.
- Harra, L.K.: 2012, The Role of Coronal Hole and Active Region Boundaries in Solar Wind Formation. In: Bellot Rubio, L., Reale, F., Carlsson, M. (eds.) *4th Hinode Science Meeting: Unsolved Problems and Recent Insights, CS-Astron. Soc. Pacific, San Francisco* **455**, 315. ADS.
- Harra, L.K., Sterling, A.C.: 2001, Material Outflows from Coronal Intensity “Dimming Regions” during Coronal Mass Ejection Onset. *Astrophys. J. Lett.* **561**, L215. DOI ADS.
- Harra, L.K., Hara, H., Imada, S., Young, P.R., Williams, D.R., Sterling, A.C., Korendyke, C., Attrill, G.D.R.: 2007, Coronal Dimming Observed with Hinode: Outflows Related to a Coronal Mass Ejection. *Pub. Astron. Soc. Japan* **59**, S801. DOI ADS.
- Harra, L.K., Sakao, T., Mandrini, C.H., Hara, H., Imada, S., Young, P.R., van Driel-Gesztelyi, L., Baker, D.: 2008, Outflows at the Edges of Active Regions: Contribution to Solar Wind Formation? *Astrophys. J. Lett.* **676**, L147. DOI ADS.
- Harra, L.K., Magara, T., Hara, H., Tsuneta, S., Okamoto, T.J., Wallace, A.J.: 2010, Response of the Solar Atmosphere to the Emergence of ‘Serpentine’ Magnetic Field. *Solar Phys.* **263**, 105. DOI ADS.
- Harra, L.K., Mandrini, C.H., Dasso, S., Gulisano, A.M., Steed, K., Imada, S.: 2011, Determining the Solar Source of a Magnetic Cloud Using a Velocity Difference Technique. *Solar Phys.* **268**, 213. DOI ADS.
- Harra, L.K., Archontis, V., Pedram, E., Hood, A.W., Shelton, D.L., van Driel-Gesztelyi, L.: 2012, The Creation of Outflowing Plasma in the Corona at Emerging Flux Regions: Comparing Observations and Simulations. *Solar Phys.* **278**, 47. DOI ADS.
- Harra, L.K., Ugarte-Urra, I., De Rosa, M., Mandrini, C., van Driel-Gesztelyi, L., Baker, D., Culhane, J.L., Démoulin, P.: 2017, A study of the long term evolution in active region upflows. *Pub. Astron. Soc. Japan* **69**, 47. DOI ADS.
- Harrison, R.A., Lyons, M.: 2000, A spectroscopic study of coronal dimming associated with a coronal mass ejection. *Astron. Astrophys.* **358**, 1097. ADS.
- Harrison, R.A., Sawyer, E.C., Carter, M.K., Cruise, A.M., Cutler, R.M., Fludra, A., Hayes, R.W., Kent, B.J., Lang, J., Parker, D.J., Payne, J., Pike, C.D., Peskett, S.C., Richards, A.G., Gulhane, J.L., Norman, K., Breeveld, A.A., Breeveld, E.R., Al Janabi, K.F., McCalden, A.J., Parkinson, J.H., Self, D.G., Thomas, P.D., Poland, A.I., Thomas, R.J.,

- Thompson, W.T., Kjeldseth-Moe, O., Brekke, P., Karud, J., Maltby, P., Aschenbach, B., Bräuning, H., Kühne, M., Hollandt, J., Siegmund, O.H.W., Huber, M.C.E., Gabriel, A.H., Mason, H.E., Bromage, B.J.I.: 1995, The Coronal Diagnostic Spectrometer for the Solar and Heliospheric Observatory. *Solar Phys.* **162**, 233. DOI ADS.
- Harrison, R.A., Bryans, P., Simnett, G.M., Lyons, M.: 2003, Coronal dimming and the coronal mass ejection onset. *Astron. Astrophys.* **400**, 1071. DOI ADS.
- Hassler, D.M., Dammasch, I.E., Lemaire, P., Brekke, P., Curdt, W., Mason, H.E., Vial, J.-C., Wilhelm, K.: 1999, Solar Wind Outflow and the Chromospheric Magnetic Network. *Science* **283**, 810. DOI ADS.
- He, J.-S., Tu, C.-Y., Marsch, E.: 2008, Modeling of Solar Wind in the Coronal Funnel with Mass and Energy Supplied at 5 Mm. *Solar Phys.* **250**, 147. DOI ADS.
- He, J.-S., Marsch, E., Tu, C.-Y., Guo, L.-J., Tian, H.: 2010, Intermittent outflows at the edge of an active region - a possible source of the solar wind? *Astron. Astrophys.* **516**, A14. DOI ADS.
- Hinode Review Team, Al-Janabi, K., Antolin, P., Baker, D., Bellot Rubio, L.R., Bradley, L., Brooks, D.H., Centeno, R., Culhane, J.L., Del Zanna, G., Doschek, G.A., Fletcher, L., Hara, H., Harra, L.K., Hillier, A.S., Imada, S., Klimchuk, J.A., Mariska, J.T., Pereira, T.M.D., Reeves, K.K., Sakao, T., Sakurai, T., Shimizu, T., Shimojo, M., Shiota, D., Solanki, S.K., Sterling, A.C., Su, Y., Suematsu, Y., Tarbell, T.D., Tiwari, S.K., Toriumi, S., Ugarte-Urra, I., Warren, H.P., Watanabe, T., Young, P.R.: 2019, Achievements of Hinode in the first eleven years. *Pub. Astron. Soc. Japan* **71**, R1. DOI ADS.
- Hudson, H.S., Acton, L.W., Freeland, S.L.: 1996, A Long-Duration Solar Flare with Mass Ejection and Global Consequences. *Astrophys. J.* **470**, 629. DOI ADS.
- Imada, S., Hara, H., Watanabe, T., Kamio, S., Asai, A., Matsuzaki, K., Harra, L.K., Mariska, J.T.: 2007, Discovery of a Temperature-Dependent Upflow in the Plage Region During a Gradual Phase of the X-Class Flare. *Pub. Astron. Soc. Japan* **59**, S793. DOI ADS.
- Janardhan, P., Tripathi, D., Mason, H.E.: 2008, The solar wind disappearance event of 11 May 1999: source region evolution. *Astron. Astrophys.* **488**, L1. DOI ADS.
- Jin, M., Ding, M.D., Chen, P.F., Fang, C., Imada, S.: 2009, Coronal Mass Ejection Induced Outflows Observed with Hinode/EIS. *Astrophys. J.* **702**, 27. DOI ADS.
- Kamio, S., Peter, H., Curdt, W., Solanki, S.K.: 2011, Continuous upflows and sporadic downflows observed in active regions. *Astron. Astrophys.* **532**, A96. DOI ADS.
- Kiddie, G., De Moortel, I., Del Zanna, G., McIntosh, S.W., Whittaker, I.: 2012, Propagating Disturbances in Coronal Loops: A Detailed Analysis of Propagation Speeds. *Solar Phys.* **279**, 427. DOI ADS.
- Kitagawa, N., Yokoyama, T.: 2015, Electron Density of Active Region Outflows Measured by the EUV Imaging Spectrometer on board Hinode. *Astrophys. J.* **805**, 97. DOI ADS.
- Klimchuk, J.A.: 2012, The role of type II spicules in the upper solar atmosphere. *Journal of Geophysical Research (Space Physics)* **117**, A12102. DOI ADS.
- Klimchuk, J.A., Bradshaw, S.J.: 2014, Are Chromospheric Nanoflares a Primary Source of Coronal Plasma? *Astrophys. J.* **791**, 60. DOI ADS.
- Ko, Y.-K., Raymond, J.C., Zurbuchen, T.H., Riley, P., Raines, J.M., Strachan, L.: 2006, Abundance Variation at the Vicinity of an Active Region and the Coronal Origin of the Slow Solar Wind. *Astrophys. J.* **646**, 1275. DOI ADS.
- Kohl, J.L., Esser, R., Gardner, L.D., Habbal, S., Daigneau, P.S., Dennis, E.F., Nystrom, G.U., Panasyuk, A., Raymond, J.C., Smith, P.L., Strachan, L., van Ballegoijen, A.A., Noci, G., Fineschi, S., Romoli, M., Ciaravella, A., Modigliani, A., Huber, M.C.E., Antonucci, E., Benna, C., Giordano, S., Tondello, G., Nicolosi, P., Naletto, G., Pernechele, C., Spadaro, D., Poletto, G., Livi, S., von der Lühe, O., Geiss, J., Timothy, J.G., Gloeckler, G., Allegra, A., Basile, G., Brusa, R., Wood, B., Siegmund, O.H.W., Fowler, W., Fisher, R., Jhabvala, M.: 1995, The Ultraviolet Coronagraph Spectrometer for the Solar and Heliospheric Observatory. *Solar Phys.* **162**, 313. DOI ADS.
- Kojima, M., Fujiki, K., Ohmi, T., Tokumaru, M., Yokobe, A., Hakamada, K.: 1999, Low-speed solar wind from the vicinity of solar active regions. *J. Geophys. Res.* **104**, 16993. DOI ADS.
- Kosugi, T., Matsuzaki, K., Sakao, T., Shimizu, T., Sone, Y., Tachikawa, S., Hashimoto, T., Minesugi, K., Ohnishi, A., Yamada, T., Tsuneta, S., Hara, H., Ichimoto, K., Suematsu, Y., Shimojo, M., Watanabe, T., Shimada, S., Davis, J.M., Hill, L.D., Owens, J.K., Title, A.M., Culhane, J.L., Harra, L.K., Doschek, G.A., Golub, L.: 2007, The Hinode (Solar-B) Mission: An Overview. *Solar Phys.* **243**, 3. DOI ADS.

- Krishna Prasad, S., Banerjee, D., Singh, J.: 2012, Oscillations in Active Region Fan Loops: Observations from EIS/ Hinode and AIA/SDO. *Solar Phys.* **281**, 67. DOI. ADS.
- Landi, E., Hutton, R., Brage, T., Li, W.: 2020, Hinode/EIS Measurements of Active-region Magnetic Fields. *Astrophys. J.* **904**, 87. DOI. ADS.
- Lemaire, P., Wilhelm, K., Curdt, W., Schule, U., Marsch, E., Poland, A.I., Jordan, S.D., Thomas, R.J., Hassler, D.M., Vial, J.C., Kuhne, M., Huber, M.C.E., Siegmund, O.H.W., Gabriel, A., Timothy, J.G., Grewing, M.: 1997, First Results of the SUMER Telescope and Spectrometer on SOHO - II. Imagery and Data Management. *Solar Phys.* **170**, 105. DOI. ADS.
- Li, L.P., Peter, H.: 2019, Plasma injection into a solar coronal loop. *Astron. Astrophys.* **626**, A98. DOI. ADS.
- Li, W., Grumer, J., Yang, Y., Brage, T., Yao, K., Chen, C., Watanabe, T., Jönsson, P., Lundstedt, H., Hutton, R., Zou, Y.: 2015, A Novel Method to Determine Magnetic Fields in Low-density Plasma Facilitated through Accidental Degeneracy of Quantum States in Fe<sup>9+</sup>. *Astrophys. J.* **807**, 69. DOI. ADS.
- Li, W., Yang, Y., Tu, B., Xiao, J., Grumer, J., Brage, T., Watanabe, T., Hutton, R., Zou, Y.: 2016, Atomic-level Pseudo-degeneracy of Atomic Levels Giving Transitions Induced by Magnetic Fields, of Importance for Determining the Field Strengths in the Solar Corona. *Astrophys. J.* **826**, 219. DOI. ADS.
- Liewer, P.C., Neugebauer, M., Zurbuchen, T.: 2004, Characteristics of active-region sources of solar wind near solar maximum. *Solar Phys.* **223**, 209. DOI. ADS.
- Liu, S., Su, J.T.: 2014, Multi-channel observations of plasma outflows and the associated small-scale magnetic field cancellations on the edges of an active region. *Astrophys. Space Sci.* **351**, 417. DOI. ADS.
- Lörincík, J., Dudík, J., Aulanier, G., Schmieder, B., Golub, L.: 2021, Imaging Evidence for Solar Wind Outflows Originating from a Coronal Mass Ejection Footpoint. *Astrophys. J.* **906**, 62. DOI. ADS.
- Macneil, A.R., Owen, C.J., Baker, D., Brooks, D.H., Harra, L.K., Long, D.M., Wicks, R.T.: 2019, Active Region Modulation of Coronal Hole Solar Wind. *Astrophys. J.* **887**, 146. DOI. ADS.
- Mandrini, C.H., Nakwacki, M.S., Attrill, G., van Driel-Gesztelyi, L., Démoulin, P., Dasso, S., Elliott, H.: 2007, Are CME-Related Dimmings Always a Simple Signature of Interplanetary Magnetic Cloud Footpoints? *Solar Phys.* **244**, 25. DOI. ADS.
- Mandrini, C.H., Nuevo, F.A., Vásquez, A.M., Démoulin, P., van Driel-Gesztelyi, L., Baker, D., Culhane, J.L., Cristiani, G.D., Pick, M.: 2014, How Can Active Region Plasma Escape into the Solar Wind from Below a Closed Helmet Streamer? *Solar Phys.* **289**, 4151. DOI. ADS.
- Mandrini, C.H., Baker, D., Démoulin, P., Cristiani, G.D., van Driel-Gesztelyi, L., Vargas Domínguez, S., Nuevo, F.A., Vásquez, A.M., Pick, M.: 2015, Parallel Evolution of Quasi-separatrix Layers and Active Region Upflows. *Astrophys. J.* **809**, 73. DOI. ADS.
- Marsch, E., Wiegmann, T., Xia, L.D.: 2004, Coronal plasma flows and magnetic fields in solar active regions. Combined observations from SOHO and NSO/Kitt Peak. *Astron. Astrophys.* **428**, 629. DOI. ADS.
- Marsch, E., Tian, H., Sun, J., Curdt, W., Wiegmann, T.: 2008, Plasma Flows Guided by Strong Magnetic Fields in the Solar Corona. *Astrophys. J.* **685**, 1262. DOI. ADS.
- Martínez-Sykora, J., De Pontieu, B., Hansteen, V., McIntosh, S.W.: 2011, What do Spectral Line Profile Asymmetries Tell us About the Solar Atmosphere? *Astrophys. J.* **732**, 84. DOI. ADS.
- Martínez-Sykora, J., De Pontieu, B., Hansteen, V.H., Rouppe van der Voort, L., Carlsson, M., Pereira, T.M.D.: 2017, On the generation of solar spicules and Alfvénic waves. *Science* **356**, 1269. DOI. ADS.
- Mason, J.P., Woods, T.N., Caspi, A., Thompson, B.J., Hock, R.A.: 2014, Mechanisms and Observations of Coronal Dimming for the 2010 August 7 Event. *Astrophys. J.* **789**, 61. DOI. ADS.
- McIntosh, S.W.: 2009, The Inconvenient Truth About Coronal Dimmings. *Astrophys. J.* **693**, 1306. DOI. ADS.
- McIntosh, S.W., De Pontieu, B.: 2009a, High-Speed Transition Region and Coronal Upflows in the Quiet Sun. *Astrophys. J.* **707**, 524. DOI. ADS.
- McIntosh, S.W., De Pontieu, B.: 2009b, Observing Episodic Coronal Heating Events Rooted in Chromospheric Activity. *Astrophys. J. Lett.* **706**, L80. DOI. ADS.

- McIntosh, S.W., De Pontieu, B., Leamon, R.J.: 2010, The Impact of New EUV Diagnostics on CME-Related Kinematics. *Solar Phys.* **265**, 5. DOI ADS.
- McIntosh, S.W., Tian, H., Sechler, M., De Pontieu, B.: 2012, On the Doppler Velocity of Emission Line Profiles Formed in the “Coronal Contraflow” that Is the Chromosphere-Corona Mass Cycle. *Astrophys. J.* **749**, 60. DOI ADS.
- Müller, D., St. Cyr, O.C., Zouganelis, I., Gilbert, H.R., Marsden, R., Nieves-Chinchilla, T., Antonucci, E., Auchère, F., Berghmans, D., Horbury, T.S., Howard, R.A., Krucker, S., Maksimovic, M., Owen, C.J., Rochus, P., Rodriguez-Pacheco, J., Romoli, M., Solanki, S.K., Bruno, R., Carlsson, M., Fludra, A., Harra, L., Hassler, D.M., Livi, S., Louarn, P., Peter, H., Schühle, U., Teriaca, L., del Toro Iniesta, J.C., Wimmer-Schweingruber, R.F., Marsch, E., Velli, M., De Groof, A., Walsh, A., Williams, D.: 2020, The Solar Orbiter mission. Science overview. *Astron. Astrophys.* **642**, A1. DOI ADS.
- Murray, M.J., Baker, D., van Driel-Gesztelyi, L., Sun, J.: 2010, Outflows at the Edges of an Active Region in a Coronal Hole: A Signature of Active Region Expansion? *Solar Phys.* **261**, 253. DOI ADS.
- Ni, L., Ji, H., Murphy, N.A., Jara-Almonte, J.: 2020, Magnetic reconnection in partially ionized plasmas. *Proc. Royal Society A* **476**, 90867. DOI ADS.
- Nishizuka, N., Hara, H.: 2011, Spectroscopic Observations of Continuous Outflows and Propagating Waves from NOAA 10942 with Extreme Ultraviolet Imaging Spectrometer/Hinode. *Astrophys. J. Lett.* **737**, L43. DOI ADS.
- Ofman, L., Wang, T.J., Davila, J.M.: 2012, Slow Magnetosonic Waves and Fast Flows in Active Region Loops. *Astrophys. J.* **754**, 111. DOI ADS.
- Panesar, N.K., Sterling, A.C., Moore, R.L., Tiwari, S.K., De Pontieu, B., Norton, A.A.: 2018, IRIS and SDO Observations of Solar Jetlets Resulting from Network-edge Flux Cancellation. *Astrophys. J. Lett.* **868**, L27. DOI ADS.
- Patsourakos, S., Klimchuk, J.A., Young, P.R.: 2014, Core and Wing Densities of Asymmetric Coronal Spectral Profiles: Implications for the Mass Supply of the Solar Corona. *Astrophys. J.* **781**, 58. DOI ADS.
- Pereira, T.M.D., De Pontieu, B., Carlsson, M., Hansteen, V., Tarbell, T.D., Lemen, J., Title, A., Boerner, P., Hurlburt, N., Wülser, J.P., Martínez-Sykora, J., Kleint, L., Golub, L., McKillop, S., Reeves, K.K., Saar, S., Testa, P., Tian, H., Jaeggli, S., Kankelborg, C.: 2014, An Interface Region Imaging Spectrograph First View on Solar Spicules. *Astrophys. J. Lett.* **792**, L15. DOI ADS.
- Peter, H.: 2010, Asymmetries of solar coronal extreme ultraviolet emission lines. *Astron. Astrophys.* **521**, A51. DOI ADS.
- Peter, H., Judge, P.G.: 1999, On the Doppler Shifts of Solar Ultraviolet Emission Lines. *Astrophys. J.* **522**, 1148. DOI ADS.
- Peter, H., Gudiksen, B.V., Nordlund, Å.: 2004, Coronal Heating through Braiding of Magnetic Field Lines. *Astrophys. J. Lett.* **617**, L85. DOI ADS.
- Peter, H., Gudiksen, B.V., Nordlund, Å.: 2006, Forward Modeling of the Corona of the Sun and Solar-like Stars: From a Three-dimensional Magnetohydrodynamic Model to Synthetic Extreme-Ultraviolet Spectra. *Astrophys. J.* **638**, 1086. DOI ADS.
- Polito, V., De Pontieu, B., Testa, P., Brooks, D.H., Hansteen, V.: 2020, IRIS Observations of the Low-atmosphere Counterparts of Active Region Outflows. *Astrophys. J.* **903**, 68. DOI ADS.
- Rachmeler, L.A., Winebarger, A.R., Savage, S.L., Golub, L., Kobayashi, K., Vigil, G.D., Brooks, D.H., Cirtain, J.W., De Pontieu, B., McKenzie, D.E., Morton, R.J., Peter, H., Testa, P., Tiwari, S.K., Walsh, R.W., Warren, H.P., Alexander, C., Ansell, D., Beabout, B.L., Beabout, D.L., Bethge, C.W., Champey, P.R., Cheimets, P.N., Cooper, M.A., Creel, H.K., Gates, R., Gomez, C., Guillory, A., Haight, H., Hogue, W.D., Holloway, T., Hyde, D.W., Kenyon, R., Marshall, J.N., McCracken, J.E., McCracken, K., Mitchell, K.O., Ordway, M., Owen, T., Ranganathan, J., Robertson, B.A., Payne, M.J., Podgorski, W., Pryor, J., Samra, J., Sloan, M.D., Soohoo, H.A., Steele, D.B., Thompson, F.V., Thornton, G.S., Watkinson, B., Windt, D.: 2019, The High-Resolution Coronal Imager, Flight 2.1. *Solar Phys.* **294**, 174. DOI ADS.
- Raju, K.P.: 2009, Relative Velocities and Linewidths in a Coronal Hole and Outside. *Solar Phys.* **255**, 119. DOI ADS.
- Raouafi, N.-E., Stenborg, G.: 2014, Role of Transients in the Sustainability of Solar Coronal Plumes. *Astrophys. J.* **787**, 118. DOI ADS.
- Reinard, A.A., Biesecker, D.A.: 2008, Coronal Mass Ejection-Associated Coronal Dimmings. *Astrophys. J.* **674**, 576. DOI ADS.

- Roupe van der Voort, L.H.M., Rutten, R.J., Sütterlin, P., Sloover, P.J., Krijger, J.M.: 2003, La Palma observations of umbral flashes. *Astron. Astrophys.* **403**, 277. DOI ADS.
- Roupe van der Voort, L., De Pontieu, B., Pereira, T.M.D., Carlsson, M., Hansteen, V.: 2015, Heating Signatures in the Disk Counterparts of Solar Spicules in Interface Region Imaging Spectrograph Observations. *Astrophys. J. Lett.* **799**, L3. DOI ADS.
- Sakao, T., Kano, R., Narukage, N., Kotoku, J., Bando, T., DeLuca, E.E., Lundquist, L.L., Tsuneta, S., Harra, L.K., Katsukawa, Y., Kubo, M., Hara, H., Matsuzaki, K., Shimojo, M., Bookbinder, J.A., Golub, L., Korreck, K.E., Su, Y., Shibasaki, K., Shimizu, T., Nakatani, I.: 2007, Continuous Plasma Outflows from the Edge of a Solar Active Region as a Possible Source of Solar Wind. *Science* **318**, 1585. DOI ADS.
- Samanta, T., Tian, H., Yurchyshyn, V., Peter, H., Cao, W., Sterling, A., Erdélyi, R., Ahn, K., Feng, S., Utz, D., Banerjee, D., Chen, Y.: 2019, Generation of solar spicules and subsequent atmospheric heating. *Science* **366**, 890. DOI ADS.
- Scott, J.T., Martens, P.C.H., Tarr, L.: 2013, Outflows and Dark Bands at Arcade-like Active Region Core Boundaries. *Astrophys. J.* **765**, 82. DOI ADS.
- Sharma, A., Tripathi, D., Erdélyi, R., Gupta, G.R., Ahmed, G.A.: 2020, Wave amplitude modulation in fan loops as observed by AIA/SDO. *Astron. Astrophys.* **638**, A6. DOI ADS.
- Shen, Y.: 2021, Observation and Modeling of Solar Jets. *Proc. Royal Society A* **477**, 20200217. DOI ADS.
- Shimizu, T., Imada, S., Kawate, T., Ichimoto, K., Suematsu, Y., Hara, H., Katsukawa, Y., Kubo, M., Toriumi, S., Watanabe, T., Yokoyama, T., Korendyke, C.M., Warren, H.P., Tarbell, T., De Pontieu, B., Teriaca, L., Schühle, U.H., Solanki, S., Harra, L.K., Matthews, S., Fludra, A., Auchère, F., Andretta, V., Naletto, G., Zhukov, A.: 2019, The Solar-C.EUVST mission. In: *UV, X-Ray, and Gamma-Ray Space Instrumentation for Astronomy XXI, Soc. Photo-Optical Instrum. En. (SPIE)* **11118**, 1111807. DOI ADS.
- Si, R., Brage, T., Li, W., Grumer, J., Li, M., Hutton, R.: 2020, A First Spectroscopic Measurement of the Magnetic-field Strength for an Active Region of the Solar Corona. *Astrophys. J. Lett.* **898**, L34. DOI ADS.
- Skogsrud, H., Roupe van der Voort, L., De Pontieu, B.: 2016, On the Active Region Bright Grains Observed in the Transition Region Imaging Channels of IRIS. *Astrophys. J.* **817**, 124. DOI ADS.
- Slemzin, V., Harra, L., Urvov, A., Kuzin, S., Goryaev, F., Berghmans, D.: 2013, Signatures of Slow Solar Wind Streams from Active Regions in the Inner Corona. *Solar Phys.* **286**, 157. DOI ADS.
- Song, H., Yao, S.: 2020, Characteristics and applications of interplanetary coronal mass ejection composition. *Science in China E: Technological Sciences* **63**, 2171. DOI ADS.
- SPICE Consortium, Anderson, M., Appourchaux, T., Auchère, F., Aznar Cuadrado, R., Barbay, J., Baudin, F., Beardsley, S., Bocchialini, K., Borgo, B., Bruzzi, D., Buchlin, E., Burton, G., Büchel, V., Caldwell, M., Caminade, S., Carlsson, M., Curdt, W., Davenne, J., Davila, J., Deforest, C.E., Del Zanna, G., Drummond, D., Dubau, J., Dumesnil, C., Dunn, G., Eccleston, P., Fludra, A., Fredvik, T., Gabriel, A., Giunta, A., Gottwald, A., Griffin, D., Grundy, T., Guest, S., Gyo, M., Haberreiter, M., Hansteen, V., Harrison, R., Hassler, D.M., Haugan, S.V.H., Howe, C., Janvier, M., Klein, R., Koller, S., Kucera, T.A., Kouliche, D., Marsch, E., Marshall, A., Marshall, G., Matthews, S.A., McQuirk, C., Meining, S., Mercier, C., Morris, N., Morse, T., Munro, G., Parenti, S., Pastor-Santos, C., Peter, H., Piffner, D., Phelan, P., Philippon, A., Richards, A., Rogers, K., Sawyer, C., Schlatter, P., Schmutz, W., Schühle, U., Shaughnessy, B., Sidher, S., Solanki, S.K., Speight, R., Spescha, M., Szvec, N., Tamiatto, C., Teriaca, L., Thompson, W., Tosh, I., Tustain, S., Vial, J.-C., Walls, B., Waltham, N., Wimmer-Schweingruber, R., Woodward, S., Young, P., de Groof, A., Pacros, A., Williams, D., Müller, D.: 2020, The Solar Orbiter SPICE instrument. An extreme UV imaging spectrometer. *Astron. Astrophys.* **642**, A14. DOI ADS.
- Srivastava, A.K., Konkol, P., Murawski, K., Dwivedi, B.N., Mohan, A.: 2014, On Thermal-Pulse-Driven Plasma Flows in Coronal Funnels as Observed by the Hinode/ EUV Imaging Spectrometer (EIS). *Solar Phys.* **289**, 4501. DOI ADS.
- Stansby, D., Baker, D., Brooks, D.H., Owen, C.J.: 2020, Directly comparing coronal and solar wind elemental fractionation. *Astron. Astrophys.* **640**, A28. DOI ADS.
- Sterling, A.C., Hudson, H.S.: 1997, Yokoh SXT Observations of X-Ray “Dimming” Associated with a Halo Coronal Mass Ejection. *Astrophys. J. Lett.* **491**, L55. DOI ADS.

- Stucki, K., Solanki, S.K., Schühle, U., Rüedi, I., Wilhelm, K., Stenflo, J.O., Brković, A., Huber, M.C.E.: 2000, Comparison of far-ultraviolet emission lines formed in coronal holes and the quiet Sun. *Astron. Astrophys.* **363**, 1145. [ADS](#).
- Su, J.T., Liu, Y., Shen, Y.D., Liu, S., Mao, X.J.: 2012, Observation of High-speed Outflows in Coronal Loops Associated with Photospheric Magnetic Field Evolution. *Astrophys. J.* **760**, 82. [DOI](#). [ADS](#).
- Teriaca, L., Banerjee, D., Doyle, J.G.: 1999, SUMER observations of Doppler shift in the quiet Sun and in an active region. *Astron. Astrophys.* **349**, 636. [ADS](#).
- Thompson, B.J., Cliver, E.W., Nitta, N., Delannée, C., Delaboudinière, J.-P.: 2000, Coronal dimmings and energetic CMEs in April-May 1998. *Geophys. Res. Lett.* **27**, 1431. [DOI](#). [ADS](#).
- Tian, H.: 2017, Probing the solar transition region: current status and future perspectives. *Res. Astron. and Astrophys.* **17**, 110. [DOI](#). [ADS](#).
- Tian, H., McIntosh, S.W., De Pontieu, B.: 2011, The Spectroscopic Signature of Quasi-periodic Upflows in Active Region Timeseries. *Astrophys. J. Lett.* **727**, L37. [DOI](#). [ADS](#).
- Tian, H., Tu, C.-Y., Marsch, E., He, J.-S., Zhou, G.-Q.: 2008, Signature of mass supply to quiet coronal loops. *Astron. Astrophys.* **478**, 915. [DOI](#). [ADS](#).
- Tian, H., Marsch, E., Curdt, W., He, J.: 2009, Upflows in Funnel-like Legs of Coronal Magnetic Loops. *Astrophys. J.* **704**, 883. [DOI](#). [ADS](#).
- Tian, H., Tu, C., Marsch, E., He, J., Kamio, S.: 2010, The Nascent Fast Solar Wind Observed by the EUV Imaging Spectrometer on Board Hinode. *Astrophys. J. Lett.* **709**, L88. [DOI](#). [ADS](#).
- Tian, H., McIntosh, S.W., Habbal, S.R., He, J.: 2011a, Observation of High-speed Outflow on Plume-like Structures of the Quiet Sun and Coronal Holes with Solar Dynamics Observatory/Atmospheric Imaging Assembly. *Astrophys. J.* **736**, 130. [DOI](#). [ADS](#).
- Tian, H., McIntosh, S.W., De Pontieu, B., Martínez-Sykora, J., Sechler, M., Wang, X.: 2011b, Two Components of the Solar Coronal Emission Revealed by Extreme-ultraviolet Spectroscopic Observations. *Astrophys. J.* **738**, 18. [DOI](#). [ADS](#).
- Tian, H., McIntosh, S.W., Wang, T., Ofman, L., De Pontieu, B., Innes, D.E., Peter, H.: 2012a, Persistent Doppler Shift Oscillations Observed with Hinode/EIS in the Solar Corona: Spectroscopic Signatures of Alfvénic Waves and Recurring Upflows. *Astrophys. J.* **759**, 144. [DOI](#). [ADS](#).
- Tian, H., McIntosh, S.W., Xia, L., He, J., Wang, X.: 2012b, What can We Learn about Solar Coronal Mass Ejections, Coronal Dimmings, and Extreme-ultraviolet Jets through Spectroscopic Observations? *Astrophys. J.* **748**, 106. [DOI](#). [ADS](#).
- Tian, H., DeLuca, E., Reeves, K.K., McKillop, S., De Pontieu, B., Martínez-Sykora, J., Carlsson, M., Hansteen, V., Kleint, L., Cheung, M., Golub, L., Saar, S., Testa, P., Weber, M., Lemen, J., Title, A., Boerner, P., Hurlburt, N., Tarbell, T.D., Wuelser, J.P., Kankelborg, C., Jaeggli, S., McIntosh, S.W.: 2014a, High-resolution Observations of the Shock Wave Behavior for Sunspot Oscillations with the Interface Region Imaging Spectrograph. *Astrophys. J.* **786**, 137. [DOI](#). [ADS](#).
- Tian, H., DeLuca, E.E., Cranmer, S.R., De Pontieu, B., Peter, H., Martínez-Sykora, J., Golub, L., McKillop, S., Reeves, K.K., Miralles, M.P., McCauley, P., Saar, S., Testa, P., Weber, M., Murphy, N., Lemen, J., Title, A., Boerner, P., Hurlburt, N., Tarbell, T.D., Wuelser, J.P., Kleint, L., Kankelborg, C., Jaeggli, S., Carlsson, M., Hansteen, V., McIntosh, S.W.: 2014b, Prevalence of small-scale jets from the networks of the solar transition region and chromosphere. *Science* **346**, 1255711. [DOI](#). [ADS](#).
- Tripathi, D., Klimchuk, J.A.: 2013, Asymmetries in Coronal Spectral Lines and Emission Measure Distribution. *Astrophys. J.* **779**, 1. [DOI](#). [ADS](#).
- Tripathi, D., Mason, H.E., Dwivedi, B.N., del Zanna, G., Young, P.R.: 2009, Active Region Loops: Hinode/Extreme-Ultraviolet Imaging Spectrometer Observations. *Astrophys. J.* **694**, 1256. [DOI](#). [ADS](#).
- Tu, C.-Y., Zhou, C., Marsch, E., Xia, L.-D., Zhao, L., Wang, J.-X., Wilhelm, K.: 2005a, Solar Wind Origin in Coronal Funnels. *Science* **308**, 519. [DOI](#). [ADS](#).
- Tu, C.-Y., Zhou, C., Marsch, E., Wilhelm, K., Xia, L.-D., Zhao, L., Wang, J.-X.: 2005b, The Height of Solar Wind Origin in Coronal Funnels and a 3-D Scenario for Solar Wind Formation. In: Fleck, B., Zurbuchen, T.H., Lacoste, H. (eds.) *Solar Wind 11/SOHO 16, Connecting Sun and Heliosphere, SP-ESA, Noordwijk* **592**, 131. [ADS](#).
- Ugarte-Urra, I., Warren, H.P.: 2011, Temporal Variability of Active Region Outflows. *Astrophys. J.* **730**, 37. [DOI](#). [ADS](#).

- Uritsky, V.M., Davila, J.M., Viall, N.M., Ofman, L.: 2013, Measuring Temperature-dependent Propagating Disturbances in Coronal Fan Loops Using Multiple SDO/AIA Channels and the Surfing Transform Technique. *Astrophys. J.* **778**, 26. DOI ADS.
- van Driel-Gesztelyi, L., Culhane, J.L., Baker, D., Démoulin, P., Mandrini, C.H., DeRosa, M.L., Rouillard, A.P., Opitz, A., Stenborg, G., Vourlidas, A., Brooks, D.H.: 2012, Magnetic Topology of Active Regions and Coronal Holes: Implications for Coronal Outflows and the Solar Wind. *Solar Phys.* **281**, 237. DOI ADS.
- Vanninathan, K., Madjarska, M.S., Galsgaard, K., Huang, Z., Doyle, J.G.: 2015, Active region upflows. I. Multi-instrument observations. *Astron. Astrophys.* **584**, A38. DOI ADS.
- Vanninathan, K., Veronig, A.M., Dissauer, K., Temmer, M.: 2018, Plasma Diagnostics of Coronal Dimming Events. *Astrophys. J.* **857**, 62. DOI ADS.
- Velli, M., Harra, L.K., Vourlidas, A., Schwadron, N., Panasenco, O., Liewer, P.C., Müller, D., Zouganelis, I., St Cyr, O.C., Gilbert, H., Nieves-Chinchilla, T., Auchère, F., Berghmans, D., Fludra, A., Horbury, T.S., Howard, R.A., Krucker, S., Maksimovic, M., Owen, C.J., Rodríguez-Pacheco, J., Romoli, M., Solanki, S.K., Wimmer-Schweingruber, R.F., Bale, S., Kasper, J., McComas, D.J., Raouafi, N., Martinez-Pillet, V., Walsh, A.P., De Groof, A., Williams, D.: 2020, Understanding the origins of the heliosphere: integrating observations and measurements from Parker Solar Probe, Solar Orbiter, and other space- and ground-based observatories. *Astron. Astrophys.* **642**, A4. DOI ADS.
- Veronig, A.M., Gómory, P., Dissauer, K., Temmer, M., Vanninathan, K.: 2019, Spectroscopy and Differential Emission Measure Diagnostics of a Coronal Dimming Associated with a Fast Halo CME. *Astrophys. J.* **879**, 85. DOI ADS.
- Verwichte, E., Marsh, M., Foullon, C., Van Doorselaere, T., De Moortel, I., Hood, A.W., Nakariakov, V.M.: 2010, Periodic Spectral Line Asymmetries in Solar Coronal Structures from Slow Magnetoacoustic Waves. *Astrophys. J. Lett.* **724**, L194. DOI ADS.
- Wang, T., Ofman, L., Davila, J.M.: 2013, Three-dimensional Magnetohydrodynamic Modeling of Propagating Disturbances in Fan-like Coronal Loops. *Astrophys. J. Lett.* **775**, L23. DOI ADS.
- Wang, T.J., Ofman, L., Davila, J.M.: 2009, Propagating Slow Magnetoacoustic Waves in Coronal Loops Observed by Hinode/EIS. *Astrophys. J.* **696**, 1448. DOI ADS.
- Wang, T.J., Ofman, L., Davila, J.M., Mariska, J.T.: 2009, Hinode/EIS observations of propagating low-frequency slow magnetoacoustic waves in fan-like coronal loops. *Astron. Astrophys.* **503**, L25. DOI ADS.
- Wang, X., McIntosh, S.W., Curdt, W., Tian, H., Peter, H., Xia, L.-D.: 2013, Temperature dependence of ultraviolet line parameters in network and internetwork regions of the quiet Sun and coronal holes. *Astron. Astrophys.* **557**, A126. DOI ADS.
- Wang, Y.-M., Sheeley, J. N. R.: 1990, Solar Wind Speed and Coronal Flux-Tube Expansion. *Astrophys. J.* **355**, 726. DOI ADS.
- Warren, H.P., Ugarte-Urra, I., Young, P.R., Stenborg, G.: 2011, The Temperature Dependence of Solar Active Region Outflows. *Astrophys. J.* **727**, 58. DOI ADS.
- Wiegmann, T., Xia, L.D., Marsch, E.: 2005, Links between magnetic fields and plasma flows in a coronal hole. *Astron. Astrophys.* **432**, L1. DOI ADS.
- Wilhelm, K., Curdt, W., Marsch, E., Schühle, U., Lemaire, P., Gabriel, A., Vial, J.-C., Grewing, M., Huber, M.C.E., Jordan, S.D., Poland, A.I., Thomas, R.J., Kühne, M., Timothy, J.G., Hassler, D.M., Siegmund, O.H.W.: 1995, SUMER - Solar Ultraviolet Measurements of Emitted Radiation. *Solar Phys.* **162**, 189. DOI ADS.
- Wilhelm, K., Dammasch, I.E., Marsch, E., Hassler, D.M.: 2000, On the source regions of the fast solar wind in polar coronal holes. *Astron. Astrophys.* **353**, 749. ADS.
- Winebarger, A.R., Warren, H., van Ballegooijen, A., DeLuca, E.E., Golub, L.: 2002, Steady Flows Detected in Extreme-Ultraviolet Loops. *Astrophys. J. Lett.* **567**, L89. DOI ADS.
- Woods, T.N., Eparvier, F.G., Hock, R., Jones, A.R., Woodraska, D., Judge, D., Didkovsky, L., Lean, J., Mariska, J., Warren, H., McMullin, D., Chamberlin, P., Berthiaume, G., Bailey, S., Fuller-Rowell, T., Sojka, J., Tobiska, W.K., Viereck, R.: 2012, Extreme Ultraviolet Variability Experiment (EVE) on the Solar Dynamics Observatory (SDO): Overview of Science Objectives, Instrument Design, Data Products, and Model Developments. *Solar Phys.* **275**, 115. DOI ADS.
- Xia, L.D., Marsch, E., Curdt, W.: 2003, On the outflow in an equatorial coronal hole. *Astron. Astrophys.* **399**, L5. DOI ADS.
- Xia, L.D., Marsch, E., Wilhelm, K.: 2004, On the network structures in solar equatorial coronal holes. Observations of SUMER and MDI on SOHO. *Astron. Astrophys.* **424**, 1025. DOI ADS.



- Xing, C., Cheng, X., Ding, M.D.: 2020, Evolution of the Toroidal Flux of CME Flux Ropes During Eruption. *The Innovation* **1**, 100059. [DOI](#).
- Yang, Z., Bethge, C., Tian, H., Tomczyk, S., Morton, R., Del Zanna, G., McIntosh, S.W., Karak, B.B., Gibson, S., Samanta, T., He, J., Chen, Y., Wang, L.: 2020a, Global maps of the magnetic field in the solar corona. *Science* **369**, 694. [DOI](#). [ADS](#).
- Yang, Z., Tian, H., Tomczyk, S., Morton, R., Bai, X., Samanta, T., Chen, Y.: 2020b, Mapping the magnetic field in the solar corona through magnetoseismology. *Sci China Tech Sci* **63**, 2357. [DOI](#). [ADS](#).
- Young, P.R.: 2015, Dark Jets in Solar Coronal Holes. *Astrophys. J.* **801**, 124. [DOI](#). [ADS](#).
- Young, P.R., O'Dwyer, B., Mason, H.E.: 2012, Velocity Measurements for a Solar Active Region Fan Loop from Hinode/EIS Observations. *Astrophys. J.* **744**, 14. [DOI](#). [ADS](#).
- Yuan, D., Nakariakov, V.M.: 2012, Measuring the apparent phase speed of propagating EUV disturbances. *Astron. Astrophys.* **543**, A9. [DOI](#). [ADS](#).
- Zangrilli, L., Poletto, G.: 2012, A SOHO/UVCS study of coronal outflows at the edge of an active region complex. *Astron. Astrophys.* **545**, A8. [DOI](#). [ADS](#).
- Zangrilli, L., Poletto, G.: 2016, Evolution of active region outflows throughout an active region lifetime. *Astron. Astrophys.* **594**, A40. [DOI](#). [ADS](#).
- Zhang, J., Yang, S., Liu, Y., Sun, X.: 2012, Emerging Dimmings of Active Regions Observed by the Solar Dynamics Observatory. *Astrophys. J. Lett.* **760**, L29. [DOI](#). [ADS](#).
- Zhang, Q.M., Zheng, R.S.: 2020, Remote coronal dimmings related to a circular-ribbon flare. *Astron. Astrophys.* **633**, A142. [DOI](#). [ADS](#).
- Zheng, R., Chen, Y., Wang, B.: 2016, Slipping Magnetic Reconnections with Multiple Flare Ribbons during an X-class Solar Flare. *Astrophys. J.* **823**, 136. [DOI](#). [ADS](#).